Reaction Chemistry & Engineering

Investigation of support effects during ethanol steam reforming over a Ni/Sepiolite catalyst

Journal:	*Reaction Chemistry & Engineering*
Manuscript ID	RE-ART-03-2023-000181.R1
Article Type:	Paper
Date Submitted by the Author:	n/a
Complete List of Authors:	Zhurka, Marinela; University of Aberdeen, School of Engineering Anderson, James; University of Aberdeen, McCue, Alan; Univ. Aberdeen, Chemistry Lemonidou, Angeliki; Aristotle University of Thessaloniki, Chemical Engineering Kechagiopoulos, Panagiotis; University of Aberdeen,

Investigation of support effects during ethanol steam reforming over a Ni/Sepiolite catalyst†

Marinela D. Zhurka,[1] James A. Anderson,[1] Alan J. McCue,[2] Angeliki A. Lemonidou,[3] Panagiotis N. Kechagiopoulos[1]*

[1] Chemical Processes & Materials Group, School of Engineering, University of Aberdeen, Aberdeen, AB24 3UE, UK

[2] Department of Chemistry, University of Aberdeen, Aberdeen, AB24 3UE, UK

[3] Laboratory of Petrochemical Technology, Department of Chemical Engineering, Aristotle University of Thessaloniki, GR-54124 Thessaloniki, Greece

* Corresponding author: p.kechagiopoulos@abdn.ac.uk

† Electronic supplementary information (ESI) available.

Abstract

Sustainable hydrogen production can be achieved efficiently by steam reforming of bio-ethanol. The use of low-cost and abundant minerals as catalyst supports can further improve the sustainability of the process. In this work, a kinetic study of ethanol steam reforming is presented using a Ni catalyst supported on natural sepiolite. Focus is placed on probing the effect of the support on the reaction mechanism, which is found to depend on the catalyst calcination temperature and degree of hydration of the sepiolite. Results suggest the presence of more than one adsorption sites where both oxygenates and water can competitively adsorb, when the catalyst has not been exposed to temperatures higher than 500^{o}C. This bifunctional mechanism is further found to be affected by the feed Steam/Carbon ratio. Thermally pre-treating the catalyst at 550^{o}C leads to an irreversible removal of support silanol groups that hinders the adsorption of reactants on sepiolite. Hydrating the non-thermally treated catalyst prior to experiments through steam exposure enhances the density of support adsorption sites leading to kinetic performances in line with those over inert supports such as SiO_2. Steam reforming of acetaldehyde, a major product of ethanol steam reforming, is also carried out leading to similar observations, building a consistent kinetic picture of the reaction over Ni/Sepiolite.

Keywords: Ethanol steam reforming; Hydrogen production; Nickel, Sepiolite support, Reaction pathway

1. Introduction

The basis of energy production systems of the world is fossil fuels, resulting in well recognised negative environmental impact. A promising alternative to fossil fuels is hydrogen, which is a clean energy carrier and can be derived sustainably from biomass.[1] The primary source of hydrogen production is natural gas or coal, leading to high CO_2 emissions. Recent studies have shown that biomass derived oxygenated compounds are economically attractive and environmentally friendly energy sources.[2] Bio-ethanol is an ideal candidate to produce H_2 through catalytic reforming (Ethanol Steam Reforming – ESR), as it can be formed from renewable feedstocks (energy crops, forestry or agro-industry waste) via fermentation and hydrolysis procedures.[3] Further advantages of bio-ethanol relate to its low toxicity and safe handling (storage and transportation). Ethanol can further be regarded as a model compound of alcohols in the aqueous fraction of bio-oil, the liquid product of biomass pyrolysis.[4]

The main products of ESR are H_2 and CO_2 according to the overall reaction (1) seen in Table 1, with hydrogen production further influenced by the water gas shift (WGS) reaction (2). By-products can also be formed, such as methane, carbon monoxide, ethylene, acetaldehyde, acetic acid, and acetone, according to reactions (3) to (10).[5] The reaction pathways of ESR presented in the literature show significant differences, depending on catalyst[5] and operating conditions,[6] further affecting hydrogen production and product selectivities. Several research groups presented kinetic studies of ESR,[7,8] suggesting, initially, dehydrogenation (3) and dehydration reactions (8) to occur, favoured by the basic and acidic features of the catalyst, respectively, and the overall balance and strength of such sites.[9] Acetaldehyde can form methane through decarbonylation (5), which can further undergo steam reforming (6)-(7). Some catalysts reported in the literature can also promote the reaction of acetaldehyde with water to produce acetic acid (9),[10,11] which can decompose to methane and carbon dioxide (10). Transition metals also tend to form encapsulating coke through the polymerization of ethylene (13), which blocks the active sites, and filamentous coke via the Boudouard reaction (11), which does not block active sites but can lead to metal segregation from the support.[12]

Many studies have suggested Ni as a suitable metal for ethanol steam reforming due to its high activity, and low cost in comparison to noble metals.[13] Carbon deposition remains a major challenge for Ni, although the nature of the support and operating conditions can prove critical in overcoming this limitation. Thus, basic supports, high operating temperature and high steam to carbon ratio are preferred as these can reduce coking without negatively impacting activity.

Currently, the interest in catalysts supported on minerals such as olivine, dolomite, attapulgite and sepiolite has increased due to their abundance, low cost, and high surface area. Sepiolite, a phyllosilicate mineral, is an interesting catalyst support characterised by its porous inner structure and fibrous morphology. Sepiolite has been widely studied as a catalyst support for a variety of hydrotreating reactions,[14–17] where doping with potassium or lanthanum,[18] incorporating metal oxides[19] and preparing the catalyst via precipitation[20,21] have further been employed to enhance its performance. Sepiolite has also been proven recently to be a favorable support for steam reforming reactions with its structural features contributing to high adsorption capacity with high stability.[22,23] The steam reforming of bio-oil and its model compounds has specifically been reported on Ni/Sepiolite, however the focus of these works was on performance analysis and not on the elucidation of the kinetics of the reaction [24,25]. Ni supported on natural sepiolite was further shown to exhibit better activity during furfural steam reforming when compared to traditional supports (SiO_2, MgO and Al_2O_3).[26]

The present study reports on an extensive kinetic analysis of ESR over Ni/Sepiolite under a wide range of experimental conditions in a fixed bed reactor. Particular focus is placed on probing the effect of the support on the reaction mechanism, which is found to depend on the catalyst calcination temperature and degree of hydration of the sepiolite. Acetaldehyde kinetic experiments are also carried out to corroborate the findings of the work, building a consistent kinetic picture of the ESR reaction over Ni/Sepiolite.

2. Experimental

2.1. *Sample preparation*

The Ni/Sepiolite catalyst with nominal 10 wt.% Ni to the final weight of the solid was prepared by a precipitation method using $Ni(NO_3)_2.6H_2O$ (Merck, reagent grade) as precursor and untreated/fresh sepiolite (Tolsa S.A., surface area 135 $m^2\ g^{-1}$) as support. Chemical analysis of the material indicated a composition of SiO_2 (66.19 %), H_2O (15.95 %), MgO (13.16 %), Na_2O (1.71 %), Al_2O_3 (1.66 %), CaO (0.56 %), K_2O (0.41 %) and Fe_2O_3 (0.36 %). The solution of nickel nitrate was firstly added to a suspension of the support material, adjusting the pH to 3.5 by the addition of nitric acid. This solution was heated to 90ºC for 30 min before addition of an urea solution, which resulted in the controlled precipitation of nickel hydroxide over the support. The suspension was filtered after 48 h and washed repeatedly with distilled water. The sample was dried at 110ºC in air for 16 h, heat treated in a N_2 flow (100 $cm^3\ min^{-1}$) at 300ºC for 3 h and then reduced in a 3.5% H_2 in Ar flow (100 $cm^3\ min^{-1}$) at 500ºC for 5.5 h,[27] before cooling to ambient temperature in a flow of N_2 and storing. Further details are provided in previous studies.[28,29]

2.2. *Reactor setup*

The kinetic experiments were carried out in a fully automated reaction system by PID Eng & Tech (Micro Activity-effy unit). The reactants (a water/ethanol or water/acetaldehyde mixture) were fed by an HPLC pump (Gilson 307). This feed was channelled through an evaporator, operating at 150ºC, and further mixed with N_2 before entering the reactor. An internally passivated stainless steel (SS316) fixed bed reactor (9.1 mm i.d., total length 304.8 mm) was used, heated by a single-zone furnace providing an isothermal region of 5 cm. The catalyst bed was diluted with α-Al_2O_3 granules (1.5 mm average size) at 1/9 catalyst/alumina weight ratio and placed within two layers of quartz wool on top of a fitted porous plate. The α-Al_2O_3 diluent was independently verified to be inert at the test conditions. A Liquid/Gas separator was used to collect the liquid reactions products, while gas products were analysed on-line in a HP5890 GC, equipped with a TCD detector and MS-5A and HS-T columns. Liquids

were analysed offline in a Thermo Scientific TRACE 1300 GC with an FID detector and a WAXMS A column.

2.3. *Experimental conditions and parameters*

Ahead of the experiments, the catalyst was treated in situ under a flow of N_2 at 500°C for 1h, and then reduced at 500°C using a 5 % H_2 in N_2 flow of 100 cm^3 min^{-1} for 1h. Reaction temperature was varied from 300 to 600°C with a Steam/Carbon (S/C) ratio equal to 3 mol_{H_2O}/mol_C (Section 3.2) at total pressure of 1.7 bar and partial pressures of ethanol and water of 0.15 and 0.90 bar, respectively, balanced by N_2. All pressure values reported herein refer to absolute pressure, with total values measured upstream of the catalyst bed. Volumetric flowrates were all measured at normal conditions. The space time effect was examined by varying the feed flow from 97 to 330 cm^3 min^{-1}, with a S/C ratio of 3, over a fixed catalyst mass ($W/F_{t0,Eth/Acet}$ from 58 to 349 g_{cat} s $g_{Eth/Acet}^{-1}$) at 400°C and steady pressure of 1.8 bar and partial pressures of ethanol and water of 0.21 and 1.29 bar, respectively, balanced by N_2 (Section 3.3). The partial pressure of water was varied from 0.26 to 1.56 bar at a total pressure of 1.9 bar and partial pressure of ethanol of 0.13 bar at 400°C (Section 3.4.1). Correspondingly, the partial pressure of ethanol was varied from 0.06 to 0.37 bar at a total pressure of 1.9 bar and partial pressure of water of 0.74 bar at 400°C (Section 3.4.2). Additional partial pressure variation experiments were carried out at the same temperature to investigate the effect of catalyst thermal pre-treatment carrying out the latter at 550°C instead of 500°C (see Section 3.4.3 for details), and degree of hydration of the support subjecting the catalyst to a flow of steam prior testing (see Section 3.4.4 for details). The behaviour of acetaldehyde versus ethanol as a reactant was also investigated, given the recognised role of the former as an important intermediate in ESR. A mass of 80 mg Ni/Sepiolite catalyst (sieved to a 300-500 μm fraction) was used in all experiments, resulting in a catalyst bed of apparent packing density of 0.4 g/cm^3.

Standard criteria by Mears[30] and Weisz-Prater[31] were applied to ensure measurements were conducted under explicit kinetic control. Atomic C, H and O mass balance closure in all tests was in the

order of 100 ± 5 %. The results presented in the following sections are expressed in terms of the following parameters, and are further compared with thermodynamic equilibrium, calculated via Gibb's free energy minimisation within the Aspen Plus software using the Peng-Robinson equation of state.

Conversion (%): $X_{Eth/Acet} = \frac{F^{in}_{Eth/Acet} - F^{out}_{Eth/Acet}}{F^{in}_{Eth/Acet}} \times 100$

Carbon Selectivity of compound y with n carbon atoms (%): $S_c(y) = \frac{0.5nF^{out}_{y}}{F^{in}_{Eth/Acet} - F^{out}_{Eth/Acet}} \times 100$

Hydrogen yield (%): $Y_{H_2} = \frac{F^{out}_{H_2}}{mF^{in}_{Eth/Acet}} \times 100$

with m being the number of hydrogen moles produced by the oxygenate's stoichiometric steam reforming, equal to 6 and 5 for ethanol and acetaldehyde, respectively. Turnover Frequency (TOF) was defined as the moles of ethanol or acetaldehyde converted per mole of Ni active sites per second and was calculated according to the below equation:

$$TOF(s^{-1}) = \frac{X_{Eth/Acet} \cdot N^{in}_{Eth/Acet}}{w_{cat} \cdot w_{Ni} \cdot D \cdot AW_{Ni}}$$

where $N^{in}_{Eth/Acet}$ is the inlet molar flow of ethanol or acetaldehyde (mol s^{-1}), w_{cat} the catalyst weight, w_{Ni} the nominal weight composition of nickel (10%), D the metal dispersion of nickel calculated via H_2 TPD measurements (see below), and AW_{Ni} the atomic weight of nickel.

2.4. ***Characterisation of fresh catalyst samples***

TPD and TPR experiments have been conducted to characterize the metal surface of the catalyst and investigate the optimal reduction conditions, respectively. A TPDRO 1100 instrument was used with a TCD detector, with a trap bed placed before the detector to remove the moisture. Prior each experiment, samples were fully oxidised under a flow of 5% O_2 in He with a heating rate of 10 ^{o}C/min up to 600^{o}C. For the H_2-TPD analysis the samples were re-reduced in situ by a flow of H_2 at 500^{o}C for

1 h, then the system was purged with He for 20 min at 30°C. The chemisorption step took place under a flow of 10% H_2/Ar for 1 h at 100°C, before measuring the desorbed H_2 while heating until 600°C with a 10°C min^{-1} rate. Quantified H_2 desorbed was used to obtain the active metal dispersion D defined as the ratio of the number of exposed Ni surface atoms to the total number of Ni atoms present in the sample. For the TPR the samples were firstly dried at 200°C for 30 min under N_2 flow, then the system was cooled down and the temperature was increased again until 800°C with a 10°C min^{-1} temperature ramp, using a 5% H_2/N_2 flow. For Thermogravimetric Analysis (TGA) experiments, a small amount of the sample (10 to 15 mg) was placed in an Al-based sample cup of a TG 209 F3 Tarsus apparatus (NETZSGH, Germany) and heated up to 800 °C at a rate of 10 °C/min under a flow of air (50 cm^3/min). XRD patterns were obtained at room temperature on a Panalytical powder diffractometer to identify crystalline phases apparent. The diffraction patterns were recorded over an angular range of $10^o<2\theta<90^o$ with a step-size of 0.013°. A BET surface area analyser Micromeritics Tristar 3000 was used to determine the total surface area of solid samples by using N_2 as adsorbate at liquid nitrogen temperature. Prior all characterisation analyses, fresh reduced samples were thermally treated under a flow of N_2 at 500°C (or 550°C) to simulate the procedures followed during catalytic testing.

3. Results and Discussion

3.1. *Characterization of Ni/Sepiolite catalyst and sepiolite*

3.1.1. Hydrogen temperature programmed reduction (H_2-TPR)

The reduction behavior of Ni/Sepiolite catalysts thermally treated at 500°C and 550°C under N_2 was studied by TPR (Figure 1). The catalyst treated at 500°C presents 3 peaks at 430°C, 620°C and 750°C, which reflect the interaction of nickel with different components of the support. Specifically, the peak at 430°C corresponds to the reduction of NiO interacting with silica,[26,32,33] the peak at 620°C is associated with the reduction of NiO-MgO on the surface and the peak at 750°C relates to the reduction of NiO-MgO in the bulk.[34,35] Regarding the Ni/Sepiolite catalyst treated at higher temperature (550°C), a minor impact on the reduction temperatures is observed with similar peaks

178 appearing at 450°C, 630°C and 740°C. Based on the obtained TPR results and considering that before
179 experimental testing the catalyst was reduced at 500°C, the degree of Ni reduction was estimated to
180 be 49% and 51% for the sample thermally treated at 500°C and 550°C, respectively. These values differ
181 slightly to that obtained in prior work via isothermal reduction at 400°C (58%),[29] however, given the
182 consistent pre-treatment of the catalyst throughout experimental testing in the present work, it is
183 important that all measurements were carried out at identical initial conditions and, hence, degree of
184 reduction. Pre-reduction was carried out at these conditions to avoid collapse of the sepiolite
185 structure at higher temperatures, as discussed in following sections. Higher reduction temperature of
186 600°C has been tested previously, leading to a higher degree of reduction (95%),[29] however, at
187 concurrent significant structural modifications.

188 3.1.2. **Hydrogen temperature programmed desorption (H_2-TPD)**

189 The H_2-TPD profiles of Ni/Sepiolite catalysts treated at 500°C and 550°C under N_2 are shown in Figure
190 2. Both samples presented three peaks at 85°C, 430°C and 540°C, with the low-temperature peak
191 corresponding to physical adsorption of hydrogen, and the high-temperature peaks originating from
192 chemisorbed hydrogen. Section S1.1 in the Electronic Supplementary Information (ESI) presents the
193 detailed quantification of the TPD data. The Ni dispersion of the catalyst subjected to 500°C was
194 calculated to be 9.3%, while an increase in thermal pre-treatment temperature to 550°C led to a slight
195 decrease of the dispersion (7.4%) suggesting limited sintering of the metal particles. Considering that
196 the reduction of the catalyst prior the desorption step was carried out at 500°C (same as that applied
197 prior experimental testing), the amount of H_2 desorbed refers to the number of Ni sites exposed during
198 the actual experiments.

199 3.1.3. **Thermal gravimetric analysis (TGA)**

200 The thermal stability of sepiolite and Ni/Sepiolite, both thermally treated at 500°C, was investigated
201 by thermogravimetric analysis (TGA). Section S1.2 in the ESI presents the detailed analysis of the
202 thermograms of the samples, while this section summarizes the main findings. For both samples, five

stepwise weight losses were identified assigned: i. to the loss of adsorbed and some zeolitic water up to approximately 150°C, ii. to the removal of the rest of the zeolitic water up to 300°C, iii. to the removal of bound water up to 530°C (causing a partial, reversible, folding in the structure of sepiolite), iv. to the dehydroxylation of sepiolite up to 670-690°C (causing the collapse of its structure), v. to the removal of the remaining hydroxyl groups up to 800°C. Ni/Sepiolite presented more loosely adsorbed water and zeolitic water, a difference attributed to the acid media used during catalyst preparation that could produce more silanol groups that could act as water adsorption sites.[29]

3.1.4. **Brunauer-Emmett-Teller (BET) surface area analysis**

Detailed BET surface area results for the Ni/Sepiolite catalyst and sepiolite are discussed in Section S1.3 in the ESI. Increasing the thermal treatment temperature of sepiolite and the Ni/Sepiolite catalyst from 300°C up to 550°C, led to a decrease of the respective BET surface and micropore areas, in line with the removal of bound water molecules demonstrated by TGA results in this temperature range. The gradual loss of coordinated water can even lead to a structural folding of the internal channels of the sepiolite, with the procedure shown to be reversible[28,29,36] or irreversible[37,38] depending on the temperature that sepiolite has been heated at (Figure S2 in the ESI).[27]Type IV adsorption-desorption isotherms of N_2 (Figure S3 in ESI) for Ni/Sepiolite and sepiolite are obtained for all samples and the temperature they were treated at, indicating the presence of some meso-porosity. Isotherms for all the samples show a Type H1 hysteresis loop corresponding to a porous structure material consisting of well-defined pore channels.[39]

3.1.5. **X-Ray Diffraction**

The crystalline phases in the sepiolite were determined by X-Ray Diffraction (XRD) after its pre-treatment at 300°C, 500°C and 550°C with Section S1.3 in the ESI presenting detailed results. Diffractograms of Ni/Sepiolite samples did not show XRD patterns for Ni, consistent with previous reports attributing this to the formation of lamellar structures during the precipitation on the Ni precursor.[27,29] The XRD analysis of sepiolite indicated its structural change with increasing

temperature, specifically the higher degree of irreversible folding of the sepiolite crystal, in agreement with BET results.

3.2. *Effect of temperature*

The effect of temperature for ESR over Ni/Sepiolite is presented in Figure 3. For all results presented in this and following sections, unless otherwise stated, the catalyst sample used has been reduced and heat treated at 500°C. Ethanol conversion increases from 13 to 58 % as temperature rises, with the hydrogen yield following closely the trend, reaching a maximum value of 46 % at the highest temperature (600 °C) studied (Figure 3a). Thermodynamics predict conversion to be 100 % at these temperatures and much higher hydrogen yield values than those experimentally observed, indicative that the results were not limited by equilibrium. Based on the high selectivities of CH_3CHO, CH_4 and CO (Figure 3c and e), it is evident that ethanol dehydrogenation and decomposition reactions dominate below 400°C. The low H_2 yield and CO_2 selectivity further indicate that ethanol reforming and water gas shift reactions do not participate significantly at these low temperatures. The increasing CH_4 selectivity up to 400°C, combined with the concurrent decreasing CO selectivity and overall low H_2 yield, indicate the presence of the methanation reaction in line with prior studies on ethanol steam reforming over Ni catalysts.[13] The increase in CO_2 selectivity and hydrogen yield, while CH_4, CO and CH_3CHO selectivities decrease as the temperature rises from 400 to 600°C, suggest the progressive promotion of WGS and reforming reactions. Trends are similar to those presented in our previous work on ESR over Ni/SiO_2,[40] indicative of the overall dominant role of the Ni metal in the reaction mechanism. To further examine this fact, the temperature effect on the steam reforming of ethanol over pure sepiolite was studied (Figure S6 in ESI). Very low conversions, below 8% were observed with selectivity to C_2H_4 being above 90% across the temperature range. Clearly, sepiolite alone cannot activate the cleavage of the C-C bond in ethanol, suggesting that operation at 450°C or higher at the presence of Ni is needed to ensure the efficient activation of reactants.

Considering that acetaldehyde is an important intermediate in the reaction pathway of ESR, acetaldehyde steam reforming (reaction (14) in Table 1) was also studied under equivalent conditions, ensuring partial pressures were the same as with the ethanol runs. As with ethanol, conversion and H_2 yield are observed to increase with temperature but are again far from thermodynamic equilibrium (Figure 3b). At temperatures higher than 450°C, acetaldehyde conversion appears to follow a different trend to that observed at lower temperatures. This could indicate that thermal decomposition of acetaldehyde is taking place, possibly upstream of the catalyst bed, resulting in the direct production of CH_4 and CO_2 in the gas phase. The changing trend in the selectivities of these two compounds at this temperature range further support this (see below.) It is worthy to note, though, the lower conversion of acetaldehyde compared to ethanol at temperature below 450°C, which indicates that the latter's conversion does not necessarily proceed via acetaldehyde, particularly considering that it is the initial C-H bond scissions towards ethoxy and acetaldehyde that are typically considered as rate-limiting.[8] Indeed, in our previous work over Ni/SiO_2[40] it was demonstrated that at temperatures over 450°C the dominant conversion pathway of ethanol most likely involves a different surface reaction intermediate, which, in an independent microkinetic modelling study from our group, was suggested to be 1-hydroxyethyl.[41] The H_2 yield achieved is approximately equal to the case of ethanol, however, given the metric's definition in acetaldehyde steam reforming reaction, this actually indicates a lower hydrogen production, as ethanol has a higher hydrogen content of 3 moles of H_2 per carbon atom compared to 2.5 for acetaldehyde.

The products of acetaldehyde steam reforming are CO, CO_2, CH_4, CH_3COCH_3 and H_2 (Figure 3d and f). The carbon selectivities of CO, CO_2 and CH_4 indicate that the reaction network shares similarities to that of ESR. Decomposition and methanation reactions are clearly favoured at the lower temperatures with WGS having low activity, as indicated by the high and opposing trends of CH_4 and CO selectivities as the temperature rises to 450°C. Reforming reactions towards hydrogen production dominate above that point, further enhanced by the WGS, clearly evident by the rising CO_2 selectivity and increasing H_2 yield. As commented above, under these conditions, where the S/C ratio is kept constant, results

suggest a prominent role of the active metal in the reaction mechanism, with Ni being a well-known methanation and steam reforming catalyst.

An important difference between ASR and ESR is the detection of acetone at measurable quantities in the liquid products of ASR. Acetone may be a product of aldol condensation of acetaldehyde to 3-hydroxybutanal (reaction (15) in Table 1),[42–44] the latter undergoing further dehydrogenation and decarboxylation to CH_3COCH_3, CO_2 and H_2 (reaction (16) in Table 1). The aldol condensation of acetaldehyde over MgO has been particularly well-examined,[45,46] while the use of sepiolite as a catalyst for condensation reactions due to its structure, consisting of octahedral sheets mainly of MgO, has also been a matter of investigation.[47] In the current work, larger amounts of acetone were observed at lower temperatures, potentially explaining also the relatively higher CO_2 selectivity in this temperature range in comparison to ESR. Nonetheless, this enhanced CO_2 productivity at low temperatures, where WGS has been demonstrated to be low in activity, could also originate from the presence of surface acetate species generated from adsorbed acetaldehyde.[48]

3.3. *Effect of space time*

The effect of contact time on the catalytic performance of ethanol and acetaldehyde steam reforming over Ni/Sepiolite at 400°C and S/C=3 is presented in Figure 4. Conversion and H_2 yield, plotted as a function of W/F (g_{cat} s g_{Eth}^{-1} and g_{cat} s g_{Acet}^{-1}) in panel a, are seen in both cases to rise with contact time. For ethanol, the conversion follows a linear trend spanning from 16 to 67% across the W/F range studied. Acetaldehyde conversion spans from 18 to 55% across the same range, however appears to follow different slopes depending on W/F value. Considering the selectivity trends discussed below, namely the very high acetone production, the varying conversion trend of acetaldehyde can be attributed to a pronounced presence of condensation reactions at the higher W/F values.

Figure 4b shows the evolution of product selectivities with varying ethanol conversion. The selectivity of CH_3CHO is seen to increase as conversion (and W/F) decreases and would clearly reach a finite value if conversion approached zero, evidence that acetaldehyde is a primary product of ESR. Opposite

303 trends are observed for CO, CO_2 and CH_4, which decrease with conversion's decrease, suggesting these
304 are secondary products. The dehydrogenation of ethanol to acetaldehyde is responsible for its primary
305 formation, while decomposition of the later or ethanol itself to CO and CH_4 and their subsequent
306 reforming and shift reactions to CO_x give rise to their secondary production. The effect of space time
307 over Ni/Sepiolite is analogous to that observed over Ni/SiO_2[40] indicative of the active metal driving the
308 overall reaction pathways under these conditions.

309 To examine the impact of the support, similar W/F variation experiments at 400°C were carried out
310 over natural sepiolite under steam reforming (Figure S7 in ESI) and decomposition (Figure S8 in ESI)
311 conditions. During decomposition, very low conversions were observed (0.5-4% depending on W/F
312 tested), well below those achieved over Ni/Sepiolite, and indicative of limited support activity in
313 activating ethanol. The only product identified was C_2H_4 suggesting that sepiolite enables the
314 dehydration of ethanol. When steam reforming was tested over natural sepiolite slightly higher
315 conversions were observed (1-6% for same W/F range), but still much lower than with Ni/Sepiolite.
316 Selectivity to C_2H_4 again was very high, above 90% across all W/F values tested. Nonetheless, traces
317 of CO_2 were also detected in the gas products, most likely originating from the gasification of carbon
318 deposits by steam, as C_2H_4 is a well-known coke precursor. In all cases, the very high selectivity to
319 ethylene is indicative of sepiolite not being able to activate the cleavage of the C-C bond in ethanol.
320 In the following sections these findings and the role of the sepiolite support in explaining observed
321 catalytic trends will be further elaborated.

322 Finally, Figure 4c presents the effect of space time on product selectivities for ASR, where significant
323 differences can be observed in relation to ESR. At lower conversion (and W/F) the selectivities of CO
324 and CH_4 are high and approximately equal at 40%. The CO/CH_4 ratio in the product stream remains
325 almost one for all space times tested, indicative of the dominant role of the acetaldehyde
326 decomposition reaction (reaction (5) in Table 1). As contact time and conversion decrease, the
327 selectivities of CO and CH_4 increase tending to non-zero values, linked to their primary formation from

acetaldehyde decomposition. In contrast, CH_3COCH_3 is clearly a secondary reaction product of ASR as its selectivity is reduced with a decrease in conversion, reaching an almost zero value at the lowest conversion studied. As discussed, its formation most likely originates from an acetaldehyde aldol condensation reaction network proceeding in parallel to ASR. Finally, the selectivity of CO_2 is influenced by the multiple pathways that involve the species, with its creation affected by acetate decomposition, acetone formation, WGS reaction and methane steam reforming reactions. Nonetheless, the decreasing trend of its selectivity as conversion decreases and the nature of the above reactions suggests CO_2 to be a secondary reaction product of ASR.

3.4. *Effect of partial pressure of reactants*

3.4.1. **Variation of water partial pressure at 400°C**

The effect of the partial pressure of water on ESR and ASR is shown in Figure 5. For these experiments, total pressure was kept constant at 1.9 bar, while the partial pressure of ethanol or acetaldehyde and total inlet flow were maintained at 0.13 bar and 213 cm^3 min^{-1}, respectively. Water partial pressure was varied between 0.26 and 1.56 bar, using N_2 as balance, resulting in a S/C variation from 1 to 6 mol_{H_2O}/mol_C. The conversion of both ethanol and acetaldehyde are positively affected by increasing water partial pressure, with H_2 yield following the conversion trend. Overall, similar conversion and H_2 yield are achieved for both reactants, although at the higher S/C ratios studied conversion of ethanol reaches greater values than the acetaldehyde. Interestingly, plotting the turnover frequency (Figure 5b) versus water partial pressure shows that both ESR and ASR exhibit positive, and approximately first order kinetics with respect to water. These findings are in contrast to the commonly reported steam-independent kinetic behaviour of ESR over Ni[49] and other metals.[50] Also in our previous work on ESR over Ni/SiO_2,[40] and Ni or Rh supported on mixed oxides of CeO_2-ZrO_2-La_2O_3[51] a slightly negative order with respect to water was observed in agreement with steam-derived intermediates not participating in the kinetically determining step. However, current results on the

Ni/Sepiolite catalyst suggest a critical role of the support in the kinetic mechanism, which appears to be consistent for both ethanol and acetaldehyde reactions.

Further evidence of support participation in the kinetic mechanism is provided by the carbon selectivities of ESR plotted against S/C variation in Figure 5c. Apart from S/C=1, where the supply of water is sub-stoichiometric for ESR, increasing the partial pressure of water and the equivalent S/C ratio is seen to lead to a decrease in the selectivity of CO_2 and conversely a rise in those of CO and CH_4. The much lower selectivity towards acetaldehyde in Figure 5c in comparison to that in Figures 3e or 4b can be attributed to the comparatively much lower partial pressure of ethanol used in these experiments. In all cases, the observed selectivity profiles contrast with the conventionally expected behaviour from an increase in the S/C ratio and the associated promotion of reforming and WGS reaction pathways.[40] The carbon selectivities observed during ASR, presented in Figure 5d, display milder trends, although still in line with the findings on ESR, with CH_4 and CO selectivities showing a slight increase at the higher S/C ratios. A complex interplay between the metal and the support is evident, where the availability of water appears to have a rate controlling influence on ethanol or acetaldehyde conversion but at the same time does not lead to a promotion of secondary reaction pathways.

These findings are tentatively attributed to the structure of sepiolite (Figure 6), consisting of six SiO_4 tetrahedra linked together to form a polymeric silica layer.[52] Between the silica layers there are MgO_6 octahedra arranged to give threefold strips leaving channels parallel to the fibre axis containing water molecules. The external surface contains OH groups originating from the exposed sides of the tetrahedral and the octahedral sheets, in the form of Si-OH and Mg-OH. Additionally, Si-OH groups are produced when the Si–O–Si bridges linking the silicate layers are broken, leaving terminal OH groups. It is known that acid media, which was used for the catalyst preparation, may attack the sepiolite structure, and is expected to increase the number of Si-OH groups.[29] These OH groups are crucial as precipitation–deposition of the nickel precursor appears to consume such hydroxyls. This preferential

reaction indicates that most, if not all, of the precursor nucleation occurs at these locations and, hence, that Ni is placed on the top part of the tetrahedral sheets and inside the open channels.[28] Indeed, the nature of the exposed metal faces was determined by infrared (IR) CO adsorption in previous work revealing the formation of layered Ni silicate precursors following precipitation and indicating the production of mostly 2D Ni (100) crystal planes on the catalyst upon reduction.[29]

Furthermore, sepiolite's hydrophilic surface is recognized as responsible for increased adsorbent behavior towards polar molecules such as water, ethanol and acetaldehyde.[53] The hydrophilicity of sepiolite depends on the high density of the silanol groups (Si-OH) that can form hydrogen bonds with the hydroxyl groups of ethanol and water.[54,55] It has indeed been suggested during phenol steam reforming on a Ni catalyst supported over mixed Ti and Zn oxides of perovskite structure that the high concentration of surface OH of the support was accountable for dual site adsorption.[56] Phenol's functional group (OH) was found to interact not only with the metal active sites but also with the surface hydroxyl groups leading to the adsorption of phenol on the support. Additionally, experimental studies on ethanol[57] and acetic acid[58] reforming on Ni/Biochar indicated that O-containing functional groups of the support could affect the catalytic performance. The ethanol decomposition and steam reforming experiments over natural sepiolite discussed in the previous section and in Figures S6 to S8 in the ESI further demonstrate the adsorption and even dehydration of ethanol on the support.

Considering the above and combined TOF and selectivity trends observed in the present work, a bifunctional mechanism is proposed that is summarized below, over two types of sites; the sepiolite surface sites (silanol groups), designated with S, and the Ni metal sites, designated with *. In the simplified network below most reactions should be considered multi-step pathways.

1. $CH_3CH_2OH/CH_3CHO + S \rightarrow CH_3CH_2OH\cdots S/CH_3CHO\cdots S$
2. $H_2O + S \rightarrow H_2O\cdots S$
3. $CH_3CH_2OH\cdots S + 2* \rightarrow CH_3CHO\cdots S + H_2 + 2*$
4. $CH_3CH_2OH\cdots S + w* \rightarrow CH_4 + CO + H_2 + w* + S$

5. $CH_3CHO\cdots S + x* \rightarrow CH_4 + CO + x* + S$
6. $CH_3CH_2OH\cdots S + H_2O\cdots S + y* \rightarrow 2CO + 4H_2 + y* + 2S$
7. $CH_3CHO\cdots S + H_2O\cdots S + z* \rightarrow 2CO + 2H_2 + z* + 2S$
8. $CO* + H_2O\cdots S + * \rightarrow CO_2 + H_2 + 2* + S$

Ethanol/acetaldehyde and water can both adsorb and activate or dissociate onto the sepiolite surface to generate C_2 and steam intermediates, respectively (steps 1 to 2). As seen in Figures S6 to S8 in the ESI, sepiolite alone is not able to activate the C-C bond. The C_2 and steam derivatives need to then migrate along the support surface to reach the metal, where a range of reactions can occur. Ethanol can further dehydrogenate to acetaldehyde with participation of metal sites (3) C-C cleavage can further occur either with ethanol and acetaldehyde dissociating to CH_4 and CO (4 and 5, respectively), or via steam reforming (6 and 7, respectively). Finally, CO from the metal sites can further react to CO_2 via the water gas shift reaction with participation from water from the support (8). Given the growth of Ni in 2D planes, it is specifically suggested that C-C cleavage and secondary reactions take place primarily at the metal-support interface, where sites of lower coordination would primarily exist. This surface diffusion of C_2 derivatives is likely driven by local concentration gradients at the periphery of the metal particles, given that C_2 consumption occurs primarily there. The proposed mechanism aligns with that for oxidative steam reforming of ethanol on Ir/CeO_2, where, similarly, surface migration of C_2 derivatives along the ceria support towards dissociation at the metal-support and interface was revealed as rate-controlling.[59] Main difference to that work is that the adsorption of ethanol/acetaldehyde and water over sepiolite is regulated by its degree of hydration and the abundance of silanol surface groups.

As the partial pressure of water increases, more water adsorbs on sepiolite's adsorption sites, eventually activating and forming steam intermediates (such as OH). The addition of water could also hydrate sepiolite's surface possibly forming new silanol groups, through the conversion of siloxane groups (Si-O-Si).[60] Therefore, this could enhance the surface diffusion of ethanol/acetaldehyde towards the metal-support interface, indicating that the migration process of the oxygenates proceeds by binding to neighbouring silanols. As a result, a higher coverage of the oxygenates occurs on the

metal-support interface, leading to higher conversion but lacking the secondary reactions like the WGS. This competitive process on the support and the interface could be responsible for the enhancement of the TOF with increasing partial pressure of water. In the case of acetaldehyde, the parallel aldol condensation pathway leading to the independent formation of CO_2 potentially further affects the observed trends.

3.4.2. Variation of ethanol/acetaldehyde partial pressure at 400°C

Figure 7a presents the effect of ethanol and acetaldehyde partial pressure on their respective conversion and H_2 yield. These experiments were conducted while keeping constant the total pressure at 1.9 bar, partial pressure of water at 0.74 bar and total inlet flow at 160 cm^3 min^{-1}, varying ethanol or acetaldehyde from 0.06 bar (S/C = 6 mol_{H_2O}/mol_C) to 0.37 (S/C = 1 mol_{H_2O}/mol_C) bar, using N_2 as balance. Given this experimental protocol, it is noted that the below experiments were carried out at varying $W/F_{Eth/Acet}$ with focus placed on manipulating partial pressures in a methodological manner. A decrease in the partial pressure of ethanol or acetaldehyde (or a respective S/C increase) was achieved by reducing the oxygenate flow, justifying the increasing trend of conversion and H_2 yield with S/C. In our previous work,[40,51] following the exact same experimental protocol and using a range of metals (Ni and Rh) and supports (SiO_2, ZrO_2-La_2O_3 and CeO_2-ZrO_2-La_2O_3), we consistently measured a positive reaction order with ethanol partial pressure. In line with several literature studies,[49,61] this trend was linked with the participation of an ethanol derived surface intermediate in the rate determining step. A similar behaviour would be expected from acetaldehyde, considering that most oxygenates, e.g., ethylene glycol,[62] and hydrocarbons, e.g., methane,[63] have been found to show similar kinetic trends during steam reforming, with acetaldehyde specifically being a major intermediate in ESR. Nonetheless, the TOF achieved (Figure 7b), shows a slightly negative order for both ethanol and acetaldehyde.

The observed trend is consistent with the observations made in the previous section, further supporting the presence of a bifunctional mechanism. In these experiments the partial pressure of

455 water was kept constant, but the increasing partial pressure of each oxygenate could promote water's
456 substitution by the ethanol/acetaldehyde on sepiolite's surface (through hydrogen bonds formed
457 between the oxygenates and the silanol groups). At high oxygenate to water ratio, a low surface
458 diffusion rate of the oxygenates towards the metal-support interface would be observed, due to the
459 discontinuous support active sites (silanols). Subsequently, a decreased coverage of the oxygenates
460 on the metal-support interface would be expected, explaining the drop in the TOF. The latter can
461 possibly also be further negatively affected by the rising availability of water to adsorb on and saturate
462 the metal active surface, as shown previously.[40] However, as the oxygenate to water ratio decreases,
463 more silanol groups are expected eventually leading to an increased coverage of the metal-support
464 interface by ethanol or acetaldehyde.

465 Figure 7c presents the carbon selectivities of ESR in terms of S/C ratio for these experiments. Similar
466 behaviour, as that discussed in Section 3.4.1, is observed, with the selectivity to CO_2 decreasing and
467 the selectivities of CH_4 and CO increasing with higher S/C. Along the lines of the previous discussion,
468 the rise of the oxygenate to water ratio leads to a lower ethanol/acetaldehyde concentration,
469 accompanied also with a high water concentration, at the metal-support interface explaining the
470 attained selectivities. In these experiments, even the sub-stoichiometric S/C=1 point follows the
471 discussed trend, which can possibly be related to the much higher partial pressure of water compared
472 to the previous experiments (0.74 bar versus 0.26 bar). For ASR carbon selectivities (Figure 7d), the
473 trends with S/C are less significant, possibly due to lower adsorption of acetaldehyde on the silanol
474 groups. However, they can still be considered to be in line with the discussed support effects, as the
475 carbonyl-containing group of acetaldehyde could also interact with the silanol groups.[64] Specifically,
476 the proposed higher active metal coverage with water as the partial pressure of the oxygenates
477 increases agrees with the rising selectivity to acetone and decreasing selectivity to CO, both linked
478 with the rise in water-derived surface intermediates.

3.4.3. **Influence of catalyst thermal pre-treatment**

The temperature is recognised as having a key effect on the dehydration of sepiolite as already discussed on the TG analysis presented on Section 3.1.3. Heating the catalysts at a temperature range between 530°C and 570°C is claimed to cause the irreversible/permanent removal of the surface silanol groups.[65] DRIFT spectra of dried unreduced sepiolite and Ni/Sepiolite collected at 100°C intervals up to 500°C have demonstrated the progressive removal of free and adjacent hydroxyls on silicon atoms.[28,29] The highest temperature that the catalyst is routinely exposed to during the previous runs is the reduction temperature and thermal treatment with N_2 both taking place at 500°C. In order to investigate the effect of the support on the reaction mechanism the catalyst sample was subjected to an in situ thermal treatment with N_2 at a temperature of 550°C for one hour instead of 500°C, effectively eliminating the surface silanol groups of the support. Following reduction at 500°C, partial pressure variation kinetic measurements at 400°C identical to Sections 3.4.1 and 3.4.2 were carried out. The impact of this thermal treatment on active nickel surface was quantified via TPD (Section 3.1.2) showing a small decrease in Ni dispersion from 9.3 to 7.4 %. The latter was considered when determining TOF values presented in the following.

Figure 8a presents the ethanol conversion and the H_2 yield achieved by varying the ethanol and water partial pressure plotted versus the S/C ratio. Decreasing the partial pressure of ethanol (increasing S/C), the ethanol conversion and H_2 yield are seen to increase steadily, whereas increasing the partial pressure of water (and S/C) resulted in a mild decrease of conversion with H_2 yield still displaying a slight rise. The results are very much in line with those using Ni/SiO_2,[40] which, given the inert support used, can be considered characteristic of metal-dominated pathways. Ethanol conversion in experiments where partial pressures were varied is overall lower than that achieved with the untreated catalyst (Figure 7a), however this can be justified by the reduced dispersion of the thermally pre-treated catalyst. The conversion achieved during experiments where the water partial pressure was varied is actually higher than that with the untreated catalyst (Figure 5a), despite the reduced active metal area, and is largely constant, evidencing the kinetic independence of the reaction to

steam and its intermediates[40] once support effects have been eliminated. This is further demonstrated by the TOF values achieved for these runs, (Figure 8b), where a positive reaction order for ethanol and a mildly negative order for water are seen, evidence of ethanol dissociation/dehydrogenation being rate limiting and catalyst surface saturation by water having a negative effect on the rate.

The TOF values obtained for all partial pressure variation experiments are further compared between each other and against those over Ni/SiO_2 (taken from Zhurka et al.[40]) in Table 2 and in graphical form in Figure S9 in the ESI. As has been shown, the thermal treatment above 540°C results in the destruction of the structure of sepiolite and the irreversible removal of surface silanol groups,[65] which should lead to reduced adsorption of reactants on sepiolite. Given the 2D growth of Ni during precipitation for the untreated catalyst, the thermal pretreatment possibly also revealed more sites of lower coordination, restructuring Ni towards 3D particles. It is important to note that the TOF obtained in these experiments, where water partial pressure was varied, is always higher than that with the untreated catalyst and only at the highest S/C is the untreated catalyst able to achieve TOF values close to those of the thermally treated sample. This is strong evidence that Ni is indeed primarily deposited on the external surface of the sepiolite, in line with the discussion in Section 3.4.1 and the observations of Anderson et al.[27] Hence, even though the thermally treated catalyst has less Ni sites due to the sintering of the metal (based on the slightly decreased Ni dispersion value), these sites are potentially of higher activity. The very similar trends and values achieved for the thermally treated catalyst in comparison to Ni/SiO_2 further support this claim.[65] Other studies where sepiolite was used as catalyst support,[22,26] have involved much higher calcination temperatures (≥ 600°C) resulting in permanent removal of surface OH.

The carbon selectivities obtained in these experiments are finally presented in Figure 8c and d, respectively. In both cases, CO_2 selectivity increased with S/C ratio while the selectivities of CH_4, CO and CH_3CHO all decreased, in very good agreement with previous works all evidencing that an excess of water favours the secondary reactions. Results are indicative of the water gas shift reaction and the

oxidation of CH_x surface species being accelerated by the abundance of steam derived intermediates, namely O and OH surface species.

3.4.4. Influence of catalyst degree of hydration

To further probe the interaction of the sepiolite support with ethanol and water under reactive conditions, a hydration pre-treatment was applied, and its impact was investigated via partial pressure variation experiments. The untreated catalyst, as used in Sections 3.4.1 and 3.4.2, following its reduction at 500°C, and prior experiments at 400°C, was exposed to a flow of 0.2 ml/min water and 50 cm^3/min N_2 at 400°C for 1 h. At reaction conditions this feed amounted to a mixture of 83% concentration of steam in N_2. Between testing each experimental condition, the catalyst was exposed again to a similar flow of steam, with all other aspects of the experiments carried out in an identical way. The conversion and H_2 yield for these experiments are shown in Figure 9a, where the higher values obtained by varying the ethanol partial pressure in comparison to the case of the thermally treated catalyst (Section 3.4.3) are clear.

More importantly, a positive order for ethanol is again obtained (Figure 9b) in contrast to the results over the untreated catalyst sample (Section 3.4.2), further supporting the proposal that in the experiments over the untreated catalyst the decreased silanol group concentration on sepiolite's surface is determining the performance. The pre-treatment procedure led to a high degree of hydration of sepiolite's surface, increasing the concentration of silanol groups, enhancing surface diffusion of the oxygenates towards the metal-support interface, where C-C bond scission and reforming reactions occur. For the case of the water partial pressure variation experiments, a positive order is still obtained over the hydrated catalyst (Figure 9b), but with a much milder slope in comparison to the untreated catalyst. Potentially, the hydration process led to increased adsorption and activation of steam, or the high partial pressure of ethanol used in these runs was still able to displace a small fraction of the water. Nonetheless, as also seen in Table 2 the TOF values obtained

554 are in the range of the thermally treated catalyst and even closer to those over Ni/SiO_2, hence again
555 strongly indicate that ethanol activation is proceeding largely unhindered.

556 Selectivities obtained further support these observations, (Figure 9c and d), since in both experiments
557 where partial pressure is varied CO_2 selectivity is found to increase, whereas CH_4 and CO selectivities
558 are seen to decrease, again in agreement with a mechanism where secondary reactions are promoted
559 by steam derived intermediates. It can be concluded that the hydration procedure resulted in the
560 enhancement of the surface diffusion of the oxygenates onto sepiolite's surface towards the metal-
561 support interface, at the same time preventing catalyst particle sintering, achieving as such optimal
562 catalytic performance both in terms of selectivity and TOF.

563 ## 4. Conclusions

564 Kinetic measurements of the ethanol and acetaldehyde steam reforming reactions over a Ni/Sepiolite
565 catalyst were carried out at a wide variety of operating conditions. Results obtained over catalyst
566 samples supported on natural sepiolite and exposed to temperatures up to 500^{o}C suggested a critical
567 role of the support. A positive reaction order for water and a negative reaction order for both ethanol
568 and acetaldehyde were obtained, in contrast to conventional observations on other hydrocarbons and
569 oxygenates reforming. A bifunctional mechanism was proposed with both steam and oxygenates
570 being able to adsorb on the support, namely on sepiolite silanol groups. The abundance of the latter
571 was further suggested to influence surface diffusion of the oxygenates towards the active metal.
572 Results over catalyst samples subjected to thermal, or hydration pre-treatment processes
573 corroborated this conclusion. In both cases, a positive reaction order for the oxygenate and an almost
574 zero reaction order for water were obtained in line with metal dominated pathways over inert
575 supports. Thermal pre-treatment at 550^{o}C or above leads to the removal of surface silanol groups,
576 preventing the adsorption of the reactants on the support. Through the full hydration of sepiolite
577 before each experiment the increase of surface silanol groups was suggested to enhance the surface
578 diffusion of the oxygenates towards the metal-support interface. TOF values obtained with pre-

579 treated catalyst samples are higher than the untreated cases and similar to those obtained with inert
580 SiO_2 supported Ni, further concluding that the majority of Ni is deposited on the external surface of
581 sepiolite and not in its channels. Finally, ethanol and acetaldehyde were found to follow similar
582 reforming pathways, consisting of primary decomposition or dehydrogenation followed by secondary
583 water gas shift and reforming, with a parallel aldol condensation pathway for acetaldehyde leading
584 further to acetone formation.

585 ## Author contributions

586 MDZ: Investigation, Writing - Original Draft. JAA: Resources, Supervision. AJM: Resources, Writing -
587 Review & Editing. AAL: Resources, Writing - Review & Editing. PNK: Conceptualization, Methodology,
588 Writing - Review & Editing, Supervision.

589 ## Conflicts of interest

590 There are no conflicts to declare.

591 ## Bibliography

592 1 D. Tang, G. L. Tan, G. W. Li, J. G. Liang, S. M. Ahmad, A. Bahadur, M. Humayun, H. Ullah, A. Khan
593 and M. Bououdina, State-of-the-art hydrogen generation techniques and storage methods: A
594 critical review, *J Energy Storage*, 2023, **64**, 107196.

595 2 C. K. R. Pocha, W. Y. Chia, Silvanir, T. A. Kurniawan, K. S. Khoo and K. W. Chew, Thermochemical
596 conversion of different biomass feedstocks into hydrogen for power plant electricity
597 generation, *Fuel*, 2023, **340**, 127472.

598 3 S. H. Mohd Azhar, R. Abdulla, S. A. Jambo, H. Marbawi, J. A. Gansau, A. A. Mohd Faik and K. F.
599 Rodrigues, Yeasts in sustainable bioethanol production: A review, *Biochem Biophys Rep*, 2017,
600 **10**, 52–61.

4 M. N. Uddin, K. Techato, J. Taweekun, M. Mofijur, M. G. Rasul, T. M. I. Mahlia and S. M. Ashrafur, An overview of recent developments in biomass pyrolysis technologies, *Energies (Basel)*, 2018, **11**, 3115.

5 P. Rosha, A. Jelle and H. Ibrahim, Recent advances in hydrogen production through catalytic steam reforming of ethanol: Advances in catalytic design, *Can J Chem Eng*, 2023, 1–21.

6 W. H. Chen, P. P. Biswas, H. C. Ong, A. T. Hoang, T. B. Nguyen and C. Di Dong, A critical and systematic review of sustainable hydrogen production from ethanol/bioethanol: Steam reforming, partial oxidation, and autothermal reforming, *Fuel*, 2023, **333**, 126526.

7 S. Crowley and M. J. Castaldi, Mechanistic insights into catalytic ethanol steam reforming using isotope-labeled reactants, *Angewandte Chemie - International Edition*, 2016, **55**, 10650–10655.

8 D. Zanchet, J. B. O. Santos, S. Damyanova, J. M. R. Gallo and J. M. C. Bueno, Toward understanding metal-catalyzed ethanol reforming, *ACS Catal*, 2015, **5**, 3841–3863.

9 Y. Guan, Y. Li, R. A. van Santen, E. J. M. Hensen and C. Li, Controlling reaction pathways for alcohol dehydration and dehydrogenation over FeSBA-15 catalysts, *Catal Letters*, 2007, **117**, 18–24.

10 G. Busca, T. Montanari, C. Resini, G. Ramis and U. Costantino, Hydrogen from alcohols: IR and flow reactor studies, *Catal Today*, 2009, **143**, 2–8.

11 L. Barattini, G. Ramis, C. Resini, G. Busca, M. Sisani and U. Costantino, Reaction path of ethanol and acetic acid steam reforming over Ni-Zn-Al catalysts. Flow reactor studies, *Chemical Engineering Journal*, 2009, **153**, 43–49.

12 K. Shi, X. An, X. Wu and X. Xie, Modification strategies for enhancing anti-coking of Ni-, Co-based catalysts during ethanol steam reforming: A review, *Int J Hydrogen Energy*, 2022, **47**, 39404–39428.

13 S. Bepari and D. Kuila, Steam reforming of methanol, ethanol and glycerol over nickel-based catalysts-A review, *Int J Hydrogen Energy*, 2020, **45**, 18090–18113.

14 S. K. Maity, B. N. Srinivas, V. V. D. N. Prasad, A. Singh, G. M. Dhar and T. S. R. P. Rao, Studies on sepiolite supported hydrotreating catalysts, *Stud Surf Sci Catal*, 1998, **113**, 579–590.

15 S. Inoue, T. Takatsuka, Y. Wada, S. Nakata and T. Ono, A new concept for catalysts of asphaltene conversion, *Catal Today*, 1998, **43**, 225–232.

16 A. J. Aznar, E. Gutiérrez, P. Díaz, A. Alvarez and G. Poncelet, Silica from sepiolite: Preparation, textural properties, and use as support to catalysts, *Microporous Materials*, 1996, **6**, 105–114.

17 X. L. Zhai, M. Y. Jia and Y. S. Shen, Structure and properties of Ni/Sepiolite catalyst, *Chin J Chem*, 2005, **23**, 557–561.

18 L. Yang, H. Fang, S. Xiong, P. Liu and H. Luo, Catalytic properties of nickel/sepiolite promoted with potassium and lanthanum in adiponitrile hydrogenation under mild conditions, *Royal Society of Chemistry*, 2016, **6**, 60933–60939.

19 A. Guerrero-Torres, C. P. Jiménez-Gómez, J. A. Cecilia, C. García-Sancho, J. J. Quirante-Sánchez, J. M. Mérida-Robles and P. Maireles-Torres, Influence of the incorporation of basic or amphoteric oxides on the performance of Cu-based catalysts supported on sepiolite in furfural hydrogenation, *Catalysts*, 2019, **9**, 315.

20 D. Jovanovic, R. Radovic and L. Mares, Nickel hydrogenation catalyst for tallow hydrogenation and for the selective hydrogenation of sunflower seed oil and soybean oil, *Catal Today*, 1998, **43**, 21–28.

21 C. P. Jiménez-Gómez, J. A. Cecilia, R. Moreno-Tost and P. Maireles-Torres, Selective furfural hydrogenation to furfuryl alcohol using Cu-based catalysts Supported on clay minerals, *Top Catal*, 2017, **60**, 1040–1053.

22 T. Liang, Y. Wang, M. Chen, Z. Yang, S. Liu, Z. Zhou and X. Li, Steam reforming of phenol-ethanol to produce hydrogen over bimetallic Ni-Cu catalysts supported on sepiolite, *Int J Hydrogen Energy*, 2017, **42**, 28233–28246.

23 3,379,505, *United States Patent and Trademark Office*, 1968.

24 S. Liu, M. Chen, L. Chu, Z. Yang, C. Zhu, J. Wang and M. Chen, Catalytic steam reforming of bio-oil aqueous fraction for hydrogen production over Ni-Mo supported on modified sepiolite catalysts, *Int J Hydrogen Energy*, 2013, **38**, 3948–3955.

25 M. Chen, X. Li, Y. Wang, C. Wang, T. Liang, H. Zhang, Z. Yang, Z. Zhou and J. Wang, Hydrogen generation by steam reforming of tar model compounds using lanthanum modified Ni/sepiolite catalysts, *Energy Convers Manag*, 2019, **184**, 315–326.

26 S. Sayas and A. Chica, Furfural steam reforming over Ni-based catalysts. Influence of Ni incorporation method, *Int J Hydrogen Energy*, 2014, **39**, 5234–5241.

27 J. A. Anderson, M. T. Rodrigo, L. Daza and S. Mendioroz, Influence of the support in the selectivity of nickel/clay catalysts for vegetable oil hydrogenation, *Langmuir*, 1993, **9**, 2485–2490.

28 J. A. Anderson and M. Galan-Fereres, Precursor-support interactions in the preparation of sepiolite-supported Ni and Pd catalysts, *Clay Miner*, 1999, **34**, 57–66.

29 J. Anderson, S. Falconer and M. Galán-Fereres, Ni/sepiolite hydrogenation catalysts Part 1: Precursor–support interaction and nature of exposed metal surfaces, *Spectrochim Acta A Mol Biomol Spectrosc*, 1997, **53**, 2627–2639.

30 M. A. Vannice, *Kinetics of Catalytic Reactions*, Springer, 2005.

31 P. B. Weisz and C. D. Prater, Interpretation of measurements in experimental catalysis, *Advances in Catalysis*, 1954, **6**, 143–196.

32 G. T. Wurzler, R. C. Rabelo-Neto, L. V. Mattos, M. A. Fraga and F. B. Noronha, Steam reforming of ethanol for hydrogen production over MgO - Supported Ni-based catalysts, *Appl Catal A Gen*, 2016, **518**, 115–128.

33 F. Wang, L. Xu and W. Shi, Syngas production from CO2 reforming with methane over core-shell Ni@SiO2 catalysts, *Journal of CO2 Utilization*, 2016, **16**, 318–327.

34 S. Sayas, N. Vivó, J. F. Da Costa-Serra and A. Chica, Toluene steam reforming over nickel based catalysts, *Int J Hydrogen Energy*, 2020, In Press, Corrected Proof.

35 M. Menor, S. Sayas and A. Chica, Natural sepiolite promoted with Ni as new and efficient catalyst for the sustainable production of hydrogen by steam reforming of the biodiesel by-products glycerol, *Fuel*, 2017, **193**, 351–358.

36 Y. Grillet, J. M. Cases, M. Francois, J. Rouquerol and J. E. Poirier, Modification of the Porous Structure and Surface Area of Sepiolite Under Vacuum Thermal Treatment, *Clays Clay Miner*, 1988, **36**, 233–242.

37 C. Serna, J. L. Ahlrichs and J. M. Serratosa, Folding in sepiolite crystals, *Clays Clay Miner*, 1975, **23**, 452–457.

38 H. Nagata, S. Shimoda and T. Sudo, On dehydration of bound water of sepiolite, *Clays Clay Miner*, 1974, **22**, 285–293.

39 Z. A. Alothman, A review: Fundamental aspects of silicate mesoporous materials, *Materials*, 2012, **5**, 2874–2902.

40 M. D. Zhurka, A. A. Lemonidou, J. A. Anderson and P. N. Kechagiopoulos, Kinetic analysis of the steam reforming of ethanol over Ni/SiO2 for the elucidation of metal-dominated reaction pathways, *React. Chem. Eng.*, 2018, **3**, 883–897.

41 F. Tijani Ahmed Afolabi, C. Li and P. N. Kechagiopoulos, Microkinetic modelling and reaction pathway analysis of the steam reforming of ethanol over Ni/SiO2, *Int J Hydrogen Energy*, 2019, **44**, 22816–22830.

42 T. Nishiguchi, T. Matsumoto, H. Kanai, K. Utani, Y. Matsumura, W. J. Shen and S. Imamura, Catalytic steam reforming of ethanol to produce hydrogen and acetone, *Appl Catal A Gen*, 2005, **279**, 273–277.

43 T. Umegaki, K. Kuratani, Y. Yamada, A. Ueda, N. Kuriyama, T. Kobayashi and Q. Xu, Hydrogen production via steam reforming of ethyl alcohol over nano-structured indium oxide catalysts, *J Power Sources*, 2008, **179**, 566–570.

44 R. Padilla, M. Benito, L. Rodríguez, A. Serrano, G. Muñoz and L. Daza, Nickel and cobalt as active phase on supported zirconia catalysts for bio-ethanol reforming: Influence of the reaction mechanism on catalysts performance, *Int J Hydrogen Energy*, 2010, **35**, 8921–8928.

45 T. Yan, W. Dai, G. Wu, S. Lang, M. Hunger, N. Guan and L. Li, Mechanistic Insights into One-Step Catalytic Conversion of Ethanol to Butadiene over Bifunctional Zn-Y/Beta Zeolite, *ACS Catal*, 2018, **8**, 2760–2773.

46 G. Pomalaza, M. Capron, V. Ordomsky and F. Dumeignil, Recent Breakthroughs in the Conversion of Ethanol to Butadiene, *Catalysts*, 2016, **6**, 203.

47 A. Corma and R. M. Martín-Aranda, Alkaline-substituted sepiolites as a new type of strong base catalyst, *J Catal*, 1991, **130**, 130–137.

48 M. C. Sanchez-sanchez, R. M. N. Yerga, D. I. Kondarides, X. E. Verykios and J. L. G. Fierro, Mechanistic Aspects of the Ethanol Steam Reforming Reaction for Hydrogen Production on Pt,Ni and PtNi Catalysts Supported on γ-Al2O3, *Journal of physical chemistry*, 2010, **114**, 3873–3882.

715 49 M. Patel, T. K. Jindal and K. K. Pant, Kinetic study of steam reforming of ethanol on Ni-based
716 ceria-zirconia catalyst, *Ind Eng Chem Res*, 2013, **52**, 15763–15771.

717 50 N. R. Peela and D. Kunzru, Steam Reforming of Ethanol in a Microchannel Reactor : Kinetic
718 Study and Reactor Simulation, *Ind Eng Chem Res*, 2011, **50**, 12881–12894.

719 51 M. D. Zhurka, A. A. Lemonidou and P. N. Kechagiopoulos, Elucidation of metal and support
720 effects during ethanol steam reforming over Ni and Rh based catalysts supported on (CeO2)-
721 ZrO2-La2O3, *Catal Today*, 2020, In Press, Corrected Proof.

722 52 M. F. Brigatti, E. Galan and B. K. G. Theng, in *Developments in Clay Science*, 2006, vol. 1, pp. 19–
723 86.

724 53 H. Marsh and F. Rodríguez-Reinoso, *Activated Carbon*, 2006, vol. 2.

725 54 Y. Lv, F. Hao, P. Liu, S. Xiong and H. Luo, Improved catalytic performance of acid-activated
726 sepiolite supported nickel and potassium bimetallic catalysts for liquid phase hydrogenation of
727 1,6-hexanedinitrile, *J Mol Catal A Chem*, 2017, **426**, 15–23.

728 55 N. Volle, F. Giulieri, A. Burr, S. Pagnotta and A. M. Chaze, Controlled interactions between
729 silanol groups at the surface of sepiolite and an acrylate matrix: Consequences on the thermal
730 and mechanical properties, *Mater Chem Phys*, 2012, **134**, 417–424.

731 56 K. S. Baamran and M. Tahir, Ni-embedded TiO2-ZnTiO3 reducible perovskite composite with
732 synergistic effect of metal/support towards enhanced H2 production via phenol steam
733 reforming, *Energy Convers Manag*, 2019, **200**, 112064.

734 57 A. T. F. Afolabi, P. N. Kechagiopoulos, Y. Liu and C. Z. Li, Kinetic features of ethanol steam
735 reforming and decomposition using a biochar-supported Ni catalyst, *Fuel Processing*
736 *Technology*, 2021, **212**, 106622.

58 Y. Wang, Z. Zhang, S. Zhang, Y. Wang, S. Hu, J. Xiang and X. Hu, Steam reforming of acetic acid over Ni/biochar catalyst treated with HNO3: Impacts of the treatment on surface properties and catalytic behaviors, *Fuel*, 2020, **278**, 118341.

59 W. Cai, F. Wang, C. Daniel, A. C. Van Veen, Y. Schuurman, C. Descorme, H. Provendier, W. Shen and C. Mirodatos, Oxidative steam reforming of ethanol over Ir/CeO 2 catalysts: A structure sensitivity analysis, *J Catal*, 2012, **286**, 137–152.

60 S. L. Warring, D. A. Beattie and A. J. McQuillan, Surficial Siloxane-to-Silanol Interconversion during Room-Temperature Hydration/Dehydration of Amorphous Silica Films Observed by ATR-IR and TIR-Raman Spectroscopy, *Langmuir*, 2016, **32**, 1568–1576.

61 O. A. Olafadehan, A. A. Ayoola, O. O. Akintunde and V. O. Adeniyi, Mechanistic Kinetic Models for Steam Reforming of concentrated crude ethanol on Ni/Al_2O_3 catalyst, *Journal of Engineering Science and Technology*, 2015, **10**, 633–653.

62 M. A. Christiansen and D. G. Vlachos, Microkinetic modeling of Pt-catalyzed ethylene glycol steam reforming, *Appl Catal A Gen*, 2012, **431**, 18–24.

63 J. Wei and E. Iglesia, Isotopic and kinetic assessment of the mechanism of reactions of CH_4 with CO_2 or H_2O to form synthesis gas and carbon on nickel catalysts, *J Catal*, 2004, **224**, 370–383.

64 M. A. Natal-Santiago, J. M. Hill and J. A. Dumesic, Studies of the adsorption of acetaldehyde, methyl acetate, ethyl acetate, and methyl trifluoroacetate on silica, *J Mol Catal A Chem*, 1999, **140**, 199–214.

65 A. Torró-Palau, J. C. Fernández-García, A. C. Orgilés-Barceló, M. M. Pastor-Blas and J. M. Martín-Martínez, Structural modification of sepiolite (natural magnesium silicate) by thermal treatment: Effect on the properties of polyurethane adhesives, *Int J Adhes Adhes*, 1997, **17**, 111–119.

760

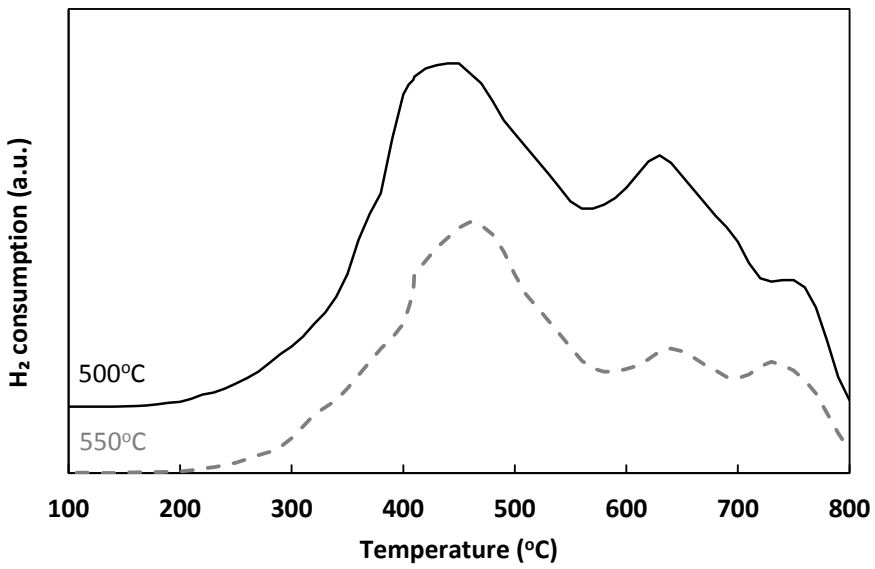

761

762 **Figure 1.** H_2-TPR measurements of Ni/Sepiolite thermally treated at 500ºC and 550ºC.

763

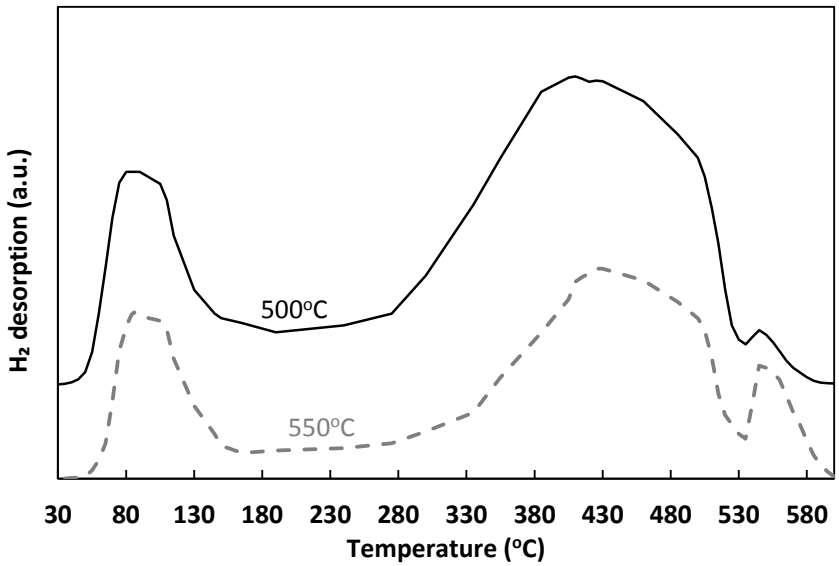

764

765 **Figure 2.** H_2-TPD profiles of Ni/Sepiolite catalyst thermally treated at 500ºC and 550ºC.

766

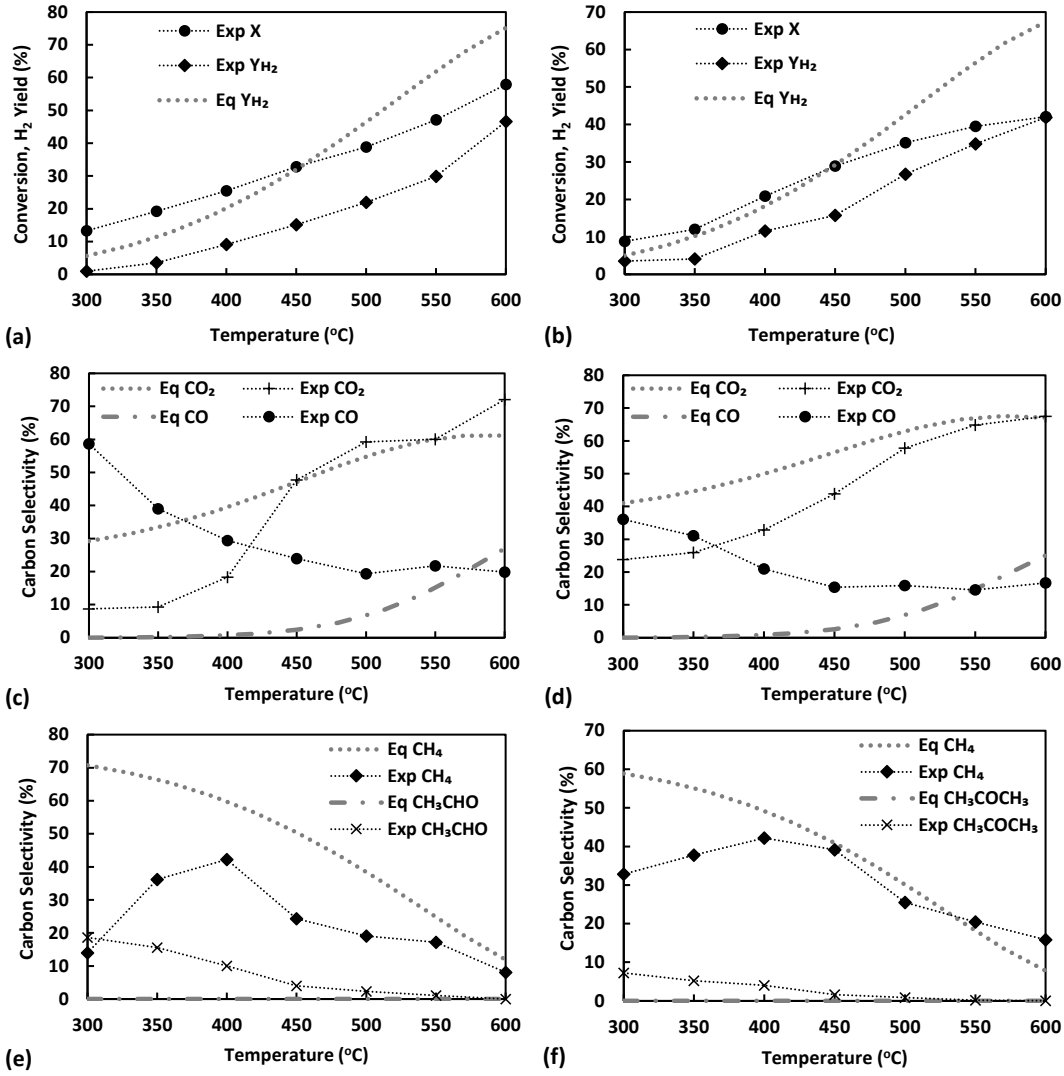

Figure 3. Temperature effect on (top) conversion and H_2 yield for ESR (a) and ASR (b), (middle) carbon selectivities of CO_2, CO for ESR (c) and ASR (d), and (bottom) carbon selectivities of CH_4 and CH_3CHO for ESR (e) and CH_4 and CH_3COCH_3 for ASR (f) compared with the equilibrium ($W/F_{Eth/Acet}$ = 91.8 g_{cat} s $g_{Eth/Acet}^{-1}$, P = 1.7 bar, S/C = 3) (lines connecting experimental points are visual aids).

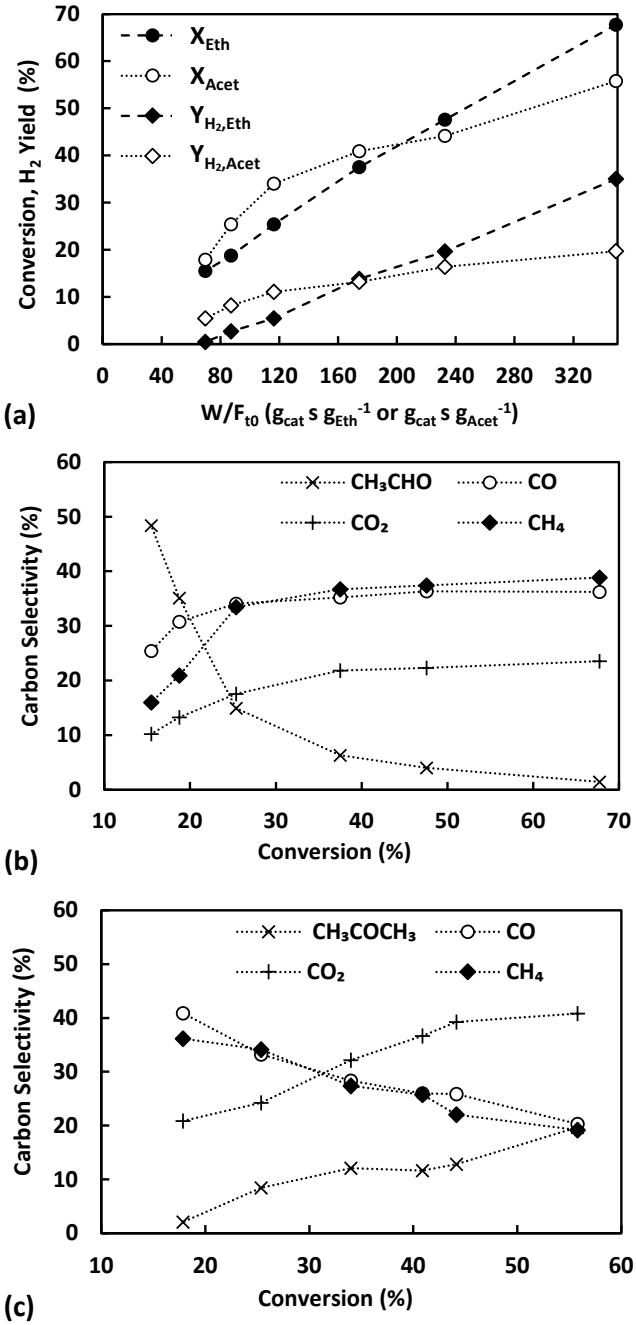

Figure 4. W/F_{t0} effect on ethanol and acetaldehyde conversion and H_2 yield at 400°C (a) and carbon selectivities of CO, CO_2, CH_4, and CH_3CHO or CH_3COCH_3 versus ethanol (b) and acetaldehyde (c) conversion. (P = 1.8 bar, S/C = 3) (lines are visual aids).

782

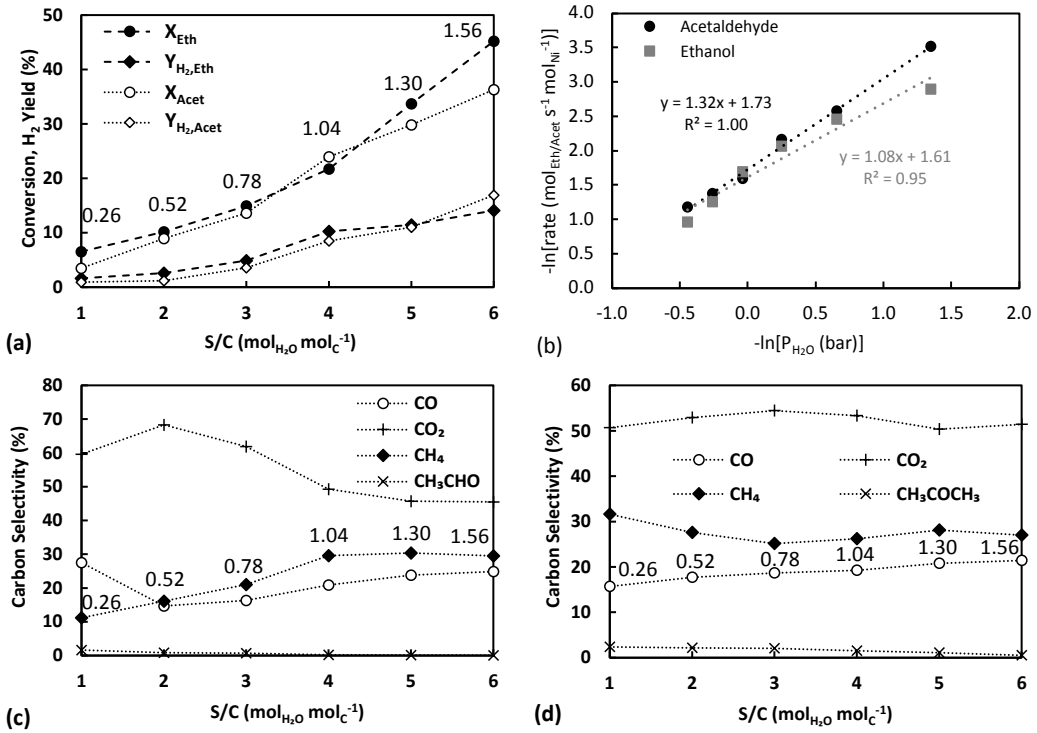

783

784

785 **Figure 5.** Partial pressure effect of water on (top) ethanol and acetaldehyde conversion and H_2 yield
786 (a) and logarithm of reaction rate of ESR and ASR with respect to logarithm of water partial pressure
787 (b), and (bottom) carbon selectivities of ESR products (c) and ASR products (d) at 400°C (P = 1.9 bar,
788 V_{tot} = 213 cm^3 min^{-1}). For panels (a), (c) and (d) the partial pressure effect is presented as a S/C
789 variation with numbers on plots annotating the equivalent partial pressures of water in bar (panels a,
790 c, and d: lines are visual aids).

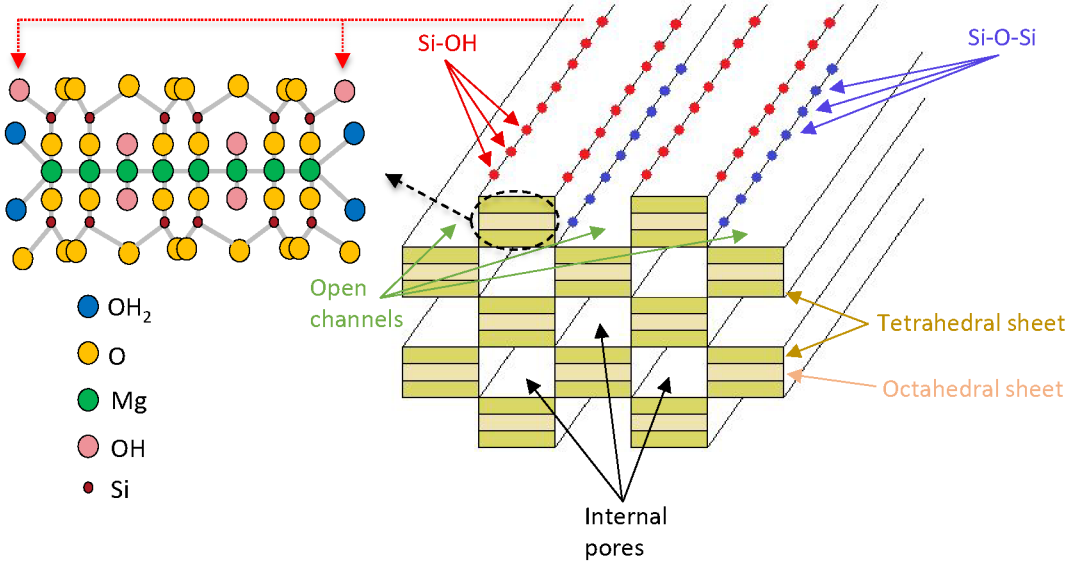

791

792 **Figure 6.** Schematic representation of sepiolite structure showing open channels, internal pores,
793 molecular and crystalline structure.

794

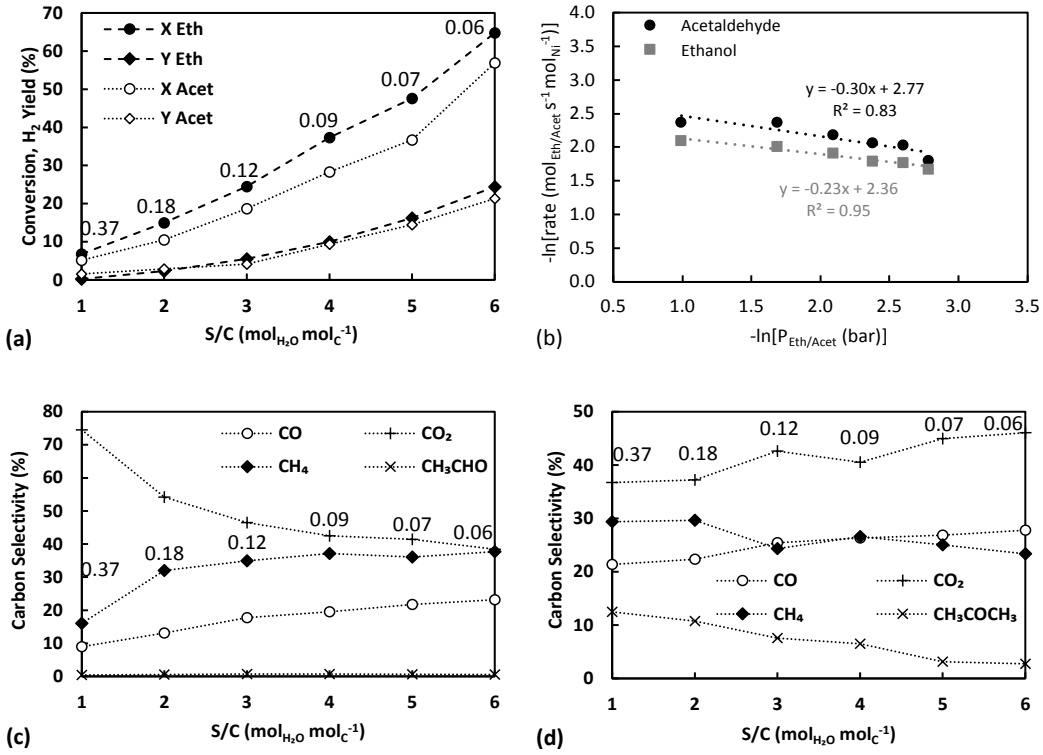

Figure 7. Partial pressure effect of ethanol and acetaldehyde on (top) the respective conversion and H_2 yield (a) and logarithm of reaction rate of ESR and ASR with respect to logarithm of ethanol and acetaldehyde partial pressure (b), and (bottom) carbon selectivities of ESR products (c) and ASR products (d) at 400°C (P = 1.9 bar, V_{tot} = 160 cm^3 min^{-1}). For panels (a), (c) and (d) the partial pressure effect is presented as a S/C variation with numbers on plots annotating the equivalent partial pressures of ethanol or acetaldehyde in bar (panels a, c, and d: lines are visual aids).

804

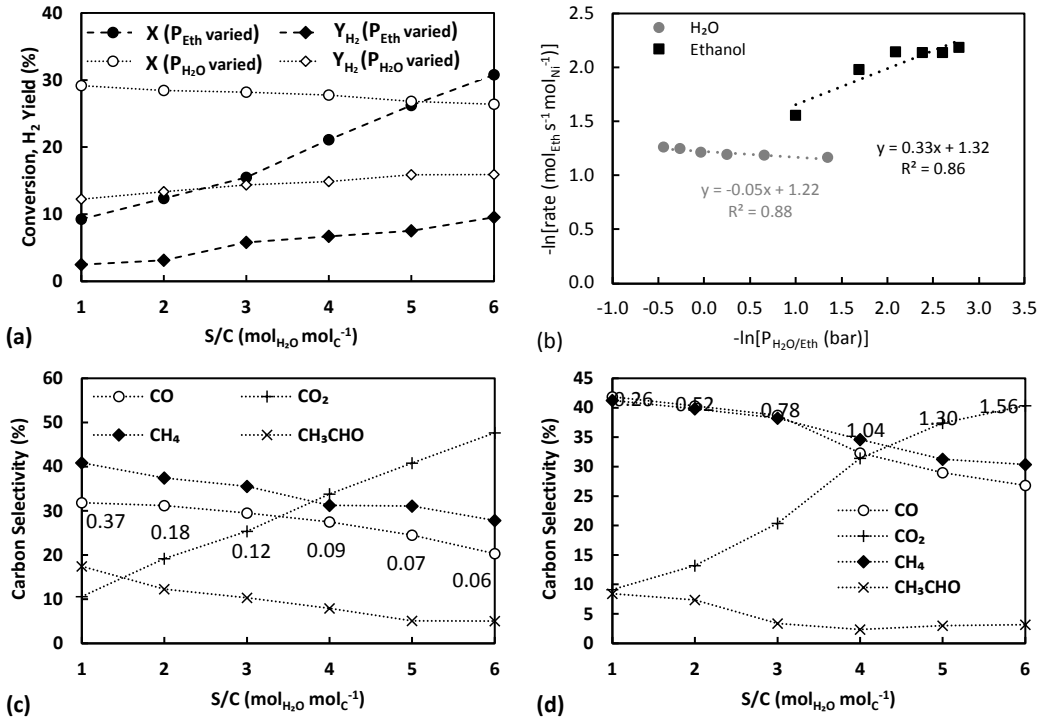

805

806 **Figure 8.** Partial pressure effect (top) of ethanol and water on the respective conversion and H_2 yield
807 (a) and logarithm of reaction rate of ESR with respect to logarithm of water and ethanol partial
808 pressure (b), and (bottom) partial pressure effect of ethanol (c) and water (d) on carbon selectivities
809 of ESR products at 400°C, on thermally pre-treated Ni/Sepiolite catalyst at 550°C (P = 1.9 bar,
810 $V_{tot}^{Ethanol}$ = 160 cm^3 min^{-1}, V_{tot}^{Water} = 213 cm^3 min^{-1}). For panels (a), (c) and (d) the partial pressure effect
811 is presented as a S/C variation with numbers on plots annotating the equivalent partial pressures of
812 ethanol or water in bar (panels a, c, and d: lines are visual aids).

813

814

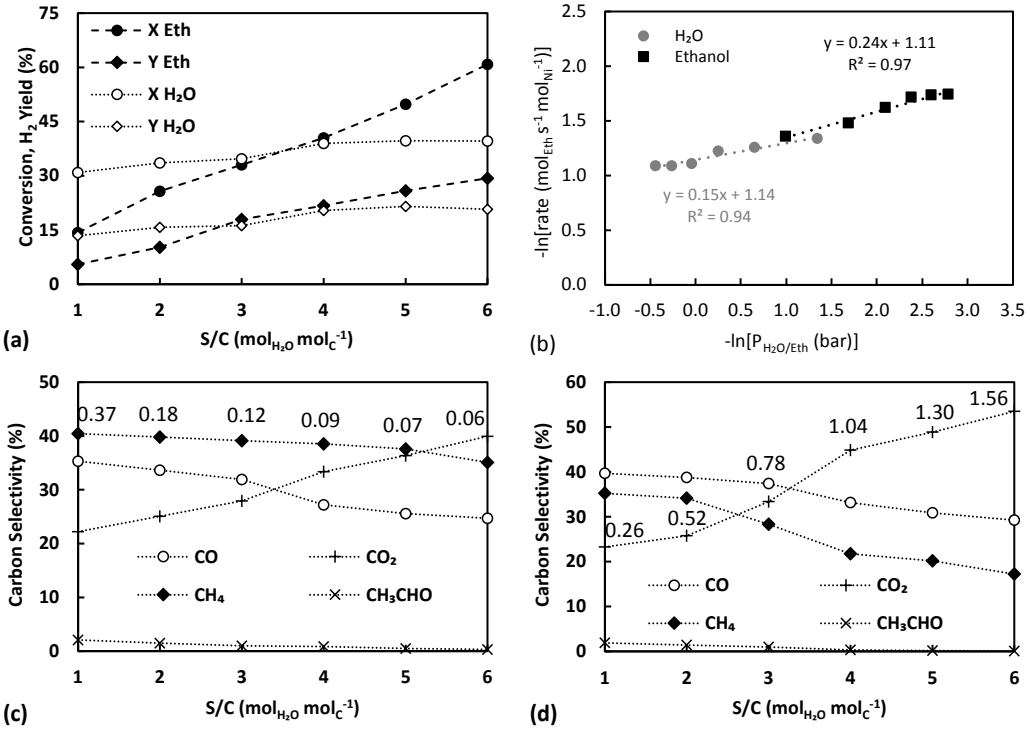

815

816 **Figure 9.** Partial pressure effect (top) of ethanol and water on the respective conversion and H_2 yield
817 (a) and logarithm of reaction rate of ESR with respect to logarithm of water and ethanol partial
818 pressure (b), and (bottom) partial pressure effect of ethanol (c) and water (d) on carbon selectivities
819 of ESR products at 400°C, on Ni/Sepiolite hydrated in situ at 400°C (P = 1.9 bar, $V_{tot}^{Ethanol}$ = 160 cm^3
820 min^{-1}, V_{tot}^{Water} = 213 cm^3 min^{-1}). For panels (a), (c) and (d) the partial pressure effect is presented as a
821 S/C variation with numbers on plots annotating the equivalent partial pressures of ethanol or water
822 in bar (panels a, c, and d: lines are visual aids).

823

824 **Table 1.** Ethanol and acetaldehyde steam reforming main reactions

(1) $CH_3CH_2OH + 3H_2O \rightleftarrows 6H_2 + 2CO_2$	(2) $CO + H_2O \rightleftarrows CO_2 + H_2$
(3) $CH_3CH_2OH \rightleftarrows CH_3CHO + H_2$	(4) $CH_3CH_2OH \rightleftarrows CH_4 + CO + H_2$
(5) $CH_3CHO \rightleftarrows CH_4 + CO$	(6) $CH_4 + H_2O \rightleftarrows CO + 3H_2$
(7) $CH_4 + 2H_2O \rightleftarrows CO_2 + 4H_2$	(8) $CH_3CH_2OH \rightleftarrows C_2H_4 + H_2O$
(9) $CH_3CHO + H_2O \rightleftarrows CH_3COOH + H_2$	(10) $CH_3COOH \rightleftarrows CH_4 + CO_2$
(11) $2CO \rightleftarrows CO_2 + C$	(12) $CH_4 \rightarrow C + 2H_2$
(13) $C_2H_4 \xrightarrow{polymerisation}$ Coke	(14) $CH_3CHO + 3H_2O \rightleftarrows 5H_2 + 2CO_2$
(15) $2CH_3CHO \rightarrow CH_3CH(OH)CH_2CHO$	(16) $CH_3CH(OH)CH_2CHO + H_2O \rightarrow CH_3COCH_3 + CO_2 + 2H_2$

825

826

827 **Table 2.** TOF values obtained during ethanol and water partial pressure variation experiments using the base case Ni/Sepiolite catalyst sample treated at
828 500°C, the thermally pre-treated sample at 550°C, and the hydrated sample at 400°C. TOF values over Ni/SiO_2 from Zhurka et al.[40] are provided for comparison.
829 P_{H_2O} variation experiments carried out at constant P_{Eth} of 0.13 bar, while P_{Eth} variation experiments carried out at constant P_{H_2O} of 0.74 bar.

P_{H_2O} (bar)	S/C	Base case	Treated at 550°C	Hydrated at 400°C	Ni/SiO_2[40]	P_{Eth} (bar)	S/C	Base case	Treated at 550°C	Hydrated at 400°C	Ni/SiO_2[40]
			(mol_{Eth} s^{-1} mol_{Ni}^{-1})						(mol_{Eth} s^{-1} mol_{Ni}^{-1})		
0.26	1	0.056	0.314	0.263	0.321	0.06	6	0.188	0.113	0.176	0.172
0.52	2	0.087	0.306	0.285	0.297	0.07	5	0.170	0.118	0.177	0.172
0.78	3	0.127	0.303	0.295	0.280	0.09	4	0.167	0.119	0.180	0.191
1.04	4	0.185	0.299	0.331	0.271	0.12	3	0.148	0.118	0.198	0.221
1.30	5	0.288	0.289	0.338	0.264	0.18	2	0.134	0.139	0.229	0.256
1.56	6	0.386	0.284	0.337	0.255	0.37	1	0.123	0.211	0.258	0.357

830

831

Supplementary Information

Investigation of support effects during ethanol steam reforming over a Ni/Sepiolite catalyst

Marinela D. Zhurka,[1] James A. Anderson,[1] Alan J. McCue,[2] Angeliki A. Lemonidou,[3] Panagiotis N. Kechagiopoulos[1]*

[1] Chemical Processes & Materials Group, School of Engineering, University of Aberdeen, Aberdeen, AB24 3UE, UK

[2] Department of Chemistry, University of Aberdeen, Aberdeen, AB24 3UE, UK

[3] Laboratory of Petrochemical Technology, Department of Chemical Engineering, Aristotle University of Thessaloniki, GR-54124 Thessaloniki, Greece

* Corresponding author: p.kechagiopoulos@abdn.ac.uk

Contents

S1. Additional characterization results

S1.1. Hydrogen temperature programmed desorption (H_2-TPD)

Table S1 presents the detailed data from the H_2 TPD measurements used for the calculation of dispersion of the Ni/Sepiolite catalyst samples thermally pre-treated at 500°C and 550°C. For the determination of exposed surface Ni sites, the dissociative adsorption of H2 is assumed, according to the reaction: $H_2 + 2M_s \rightleftarrows 2M_s - H$, resulting in a stoichiometry factor $n = 2$.

Table S1. Detailed H_2 TPD data used for the calculation of dispersion of the Ni/Sepiolite catalyst samples thermally pre-treated at different temperatures.

Pre-treatment temperature (°C)	H_2 adsorbed (mol)	Surface Ni sites (mol)	w_{cat} (mg)	Total Ni sites (mol)	Dispersion (%)
500	1.191×10^{-5}	2.382×10^{-5}	150	2.556×10^{-4}	9.32
550	9.443×10^{-6}	1.889×10^{-5}	150	2.556×10^{-4}	7.39

S1.2. Thermal gravimetric analysis (TGA)

The thermal stability of sepiolite and Ni/Sepiolite, both thermally treated at 500°C, was investigated by thermogravimetric analysis (TGA), with Figure S1 presenting the thermograms of the samples.

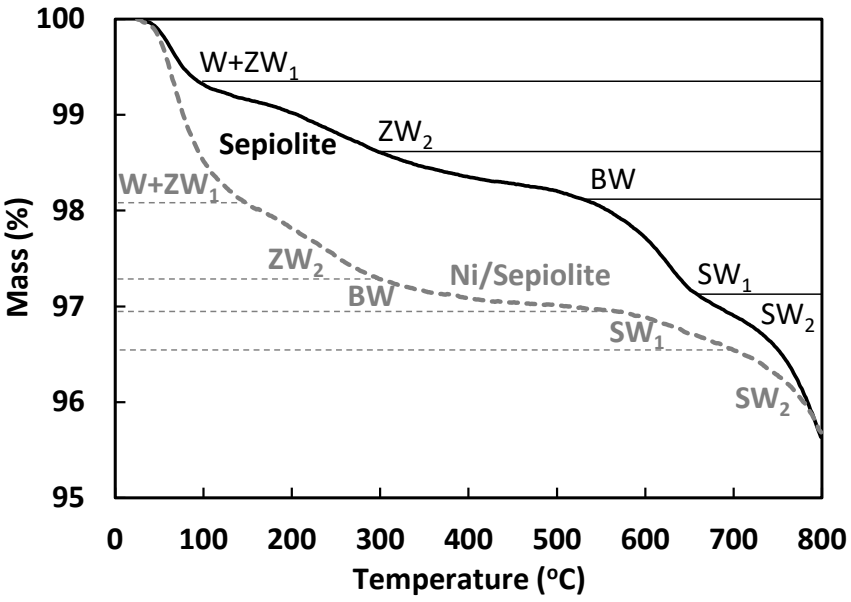

Figure S1. Thermogravimetric profiles of sepiolite and Ni/Sepiolite thermally treated at 500°C.

Both samples undergo stepwise weight loss with increasing temperature. Regarding sepiolite, observations are in agreement with results presented in various studies.[1–4] The first weight loss of 0.7% up to 100°C is assigned to the loss of all types of water - adsorbed (W) and some zeolitic (ZW_1) water. The second endothermic mass loss of 0.7% up to 300°C is due to the removal of the rest of the zeolitic water (ZW_2). It should be noted that there is no clear distinction between the dehydration temperatures of the interparticle water and the zeolitic water. The third endothermic mass loss of 0.6%, between 300°C and 530°C, relates to the removal of bound water (BW). The loss of bound water up to 530°C could cause a partial (reversible) folding in the structure of sepiolite. The fourth endothermic mass loss of 0.8% between 530°C and 670°C originates from the dehydroxylation (SW_1) of sepiolite causing the collapse of its structure. The last mass loss of 1.4% up to 800°C is attributed to the removal of remaining hydroxyl groups (structural water, SW_2). Regarding Ni/Sepiolite, as with sepiolite, five stepwise weight losses are identified with main differences observed on the associated temperatures. Specifically, the first weight loss of 1.9% concludes at 180°C, the second mass loss of 0.8% proceeds up to 300°C, the third weight loss of 0.3% occurs up to 530°C, the fourth mass loss of 0.4% completes at 690°C, while up to 800°C a further mass loss of 1% is noted. Comparing the TGA profiles of sepiolite and Ni/Sepiolite, it is observed that the latter presents more loosely adsorbed water and zeolitic water and less bounded and structural water. This difference could be attributed to the modification of sepiolite's structure during the catalyst preparation, where the acid media could alter sepiolite's surface producing more silanol groups which could act as water adsorption sites.[5]

S1.3. Brunauer-Emmett-Teller (BET) surface area analysis

The BET surface areas of Ni/Sepiolite catalyst and sepiolite are presented in Table S2. Values for 500°C and 550°C were obtained following procedures described in Section 2.4 of the main manuscript. Values at 300°C refer to the catalyst sample heat treated in a N_2 flow at 300°C but prior it being subjected to any higher temperature, namely reduction at 500°C and any subsequent thermal treatments (see Section 2.1 of the main manuscript). The data for 300°C are included for comparison and were obtained from prior works of the authors.[5,6]

Table S2. BET and micropore area of sepiolite and Ni/Sepiolite treated at 300°C (from Anderson et al.[5,6]), 500°C and 550°C.

Samples	BET area ($m^2\ g^{-1}$)			Micropore area ($m^2\ g^{-1}$)		
	300°C	500°C	550°C	300°C	500°C	550°C
Sepiolite	121	108	104	17	2	0.6
Ni/Sepiolite	157	143	133	50	42	39

The BET surface area of sepiolite thermally treated at 300°C was found to be 121 $m^2 g^{-1}$, with the micropore area found equal to 17 $m^2 g^{-1}$. Upon increasing the thermal treatment temperature up to 550°C, the BET surface area decreased to 104 $m^2 g^{-1}$, and the micropore area to 0.6 $m^2 g^{-1}$. These values are in general agreement with those reported in literature for the BET surface of sepiolite ranging between 80-350 $m^2 g^{-1}$.[7,8] As demonstrated by the TGA profiles, upon heating, sepiolite can be dehydrated, with low temperatures (below 250°C) being adequate for the removal of zeolitic water, while higher temperatures (up to about 550°C) being required for the removal of bound water molecules. The gradual loss of coordinated water can even lead to a structural folding of the internal channels of the sepiolite, with the procedure shown to be reversible[5,6,9] or irreversible[10,11] depending on the temperature that sepiolite has been heated at (Figure S2).

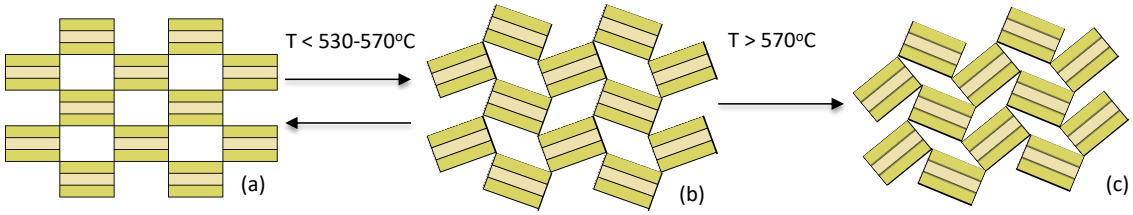

Figure S2. Schematic representation of hydrated (a), dehydrated (b) and folded (c) sepiolite structure.

Similarly, higher BET surface and micropore areas are observed for Ni/Sepiolite catalyst treated at 300°C (157 and 50 $m^2 g^{-1}$) in comparison to Ni/Sepiolite treated at 550°C (133 and 39 $m^2 g^{-1}$). Interestingly, the BET and micropore areas of Ni/Sepiolite were higher than sepiolite possibly due to the incorporation of the active phase. Similar observations were made over Ni/Clay catalysts, suggesting the increase of BET area being the result of the metal deposition via the precipitation method and associated textural changes.[12] Type IV adsorption-desorption isotherms of N_2 (Figure S3) for Ni/Sepiolite and sepiolite are obtained for all samples and the temperature they were treated at, indicating the presence of some meso-porosity. Ni/Sepiolite treated at 300°C presents the largest meso-porosity of all samples, as evidenced by the wider hysteresis loop. Isotherms for all the samples show a Type H1 hysteresis loop corresponding to a porous structure material consisting of well-defined pore channels.[13]

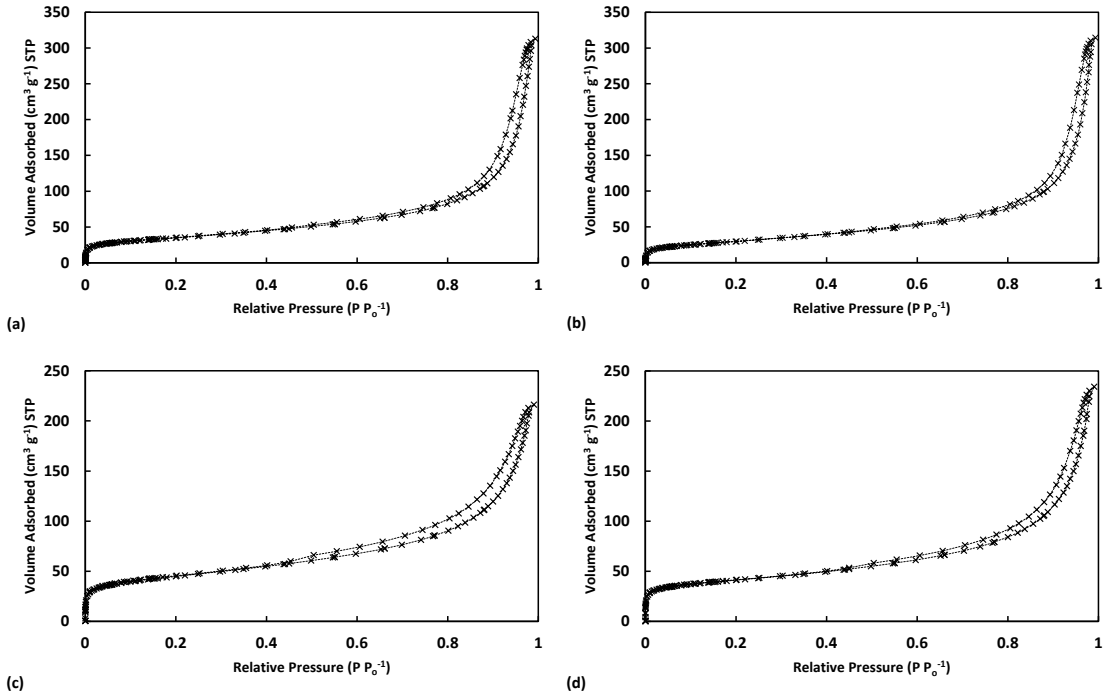

Figure S3. Adsorption-desorption isotherms of N_2 of sepiolite treated at 300°C (a) and 500°C (b) and Ni/Sepiolite treated at 300°C (c) and 500°C (d).

Pore size distribtion data presented in Figure S4 corroborate the above observations. Even though the number of data points are not enough to accurately characterize the distribution of mesopores, sepiolite samples treated at different temperatures overall show similarities between each other in terms of mesoporosity (Figure S4a), while the same holds for Ni/Sepiolite samples treated at different temperatures (Figure S4b). As such, the small differences observed between the two types of samples can be mainly attributed to the incorporation of the metal and the associated precipitation procedure applied as discussed above.

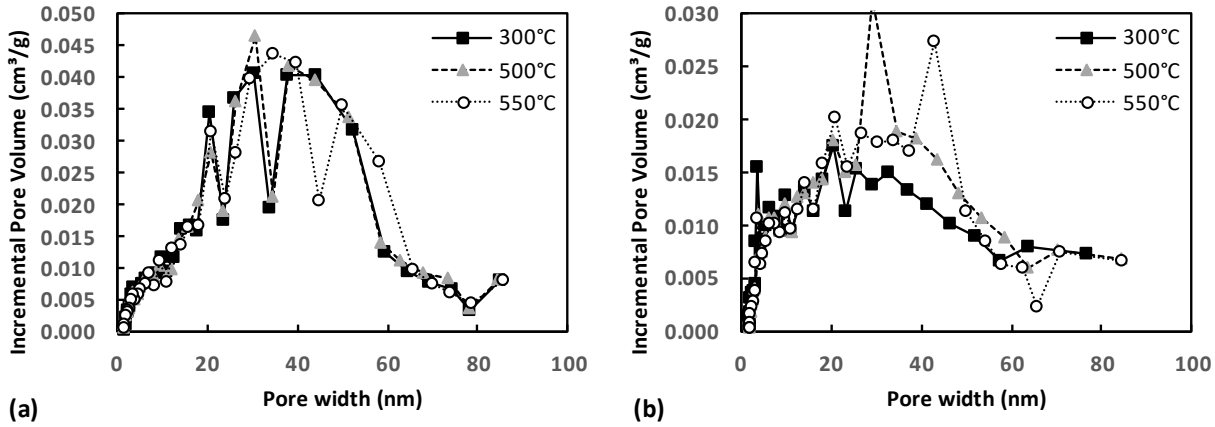

Figure S4. Pore size distribution data of sepiolite (a) and Ni/Sepiolite (b) treated at different temperatures.

S1.4. X-Ray Diffraction

The crystalline phases in the sepiolite were determined by X-Ray Diffraction (XRD) after its pre-treatment at 300°C, 500°C and 550°C, with results shown in Figure S5. Diffractograms of Ni/Sepiolite samples did not show XRD patterns for Ni, consistent with previous reports attributing this behaviour to the formation of lamellar structures during the precipitation on the Ni precursor.[5,12] The XRD analysis of sepiolite revealed that increasing the temperature from 300°C to 550°C resulted in sepiolite's structural change. Specifically, the elimination of the peak at 7.35° (1.202 nm) for the sample treated at 550°C reveals the higher degree of the irreversible folding of the sepiolite crystal, in agreement with BET results.[1] Additionally, the slight increase in the peak at 8.9°, with a simultaneous reduction of the d-spacing from 1.030 to 1.024 nm, indicated the formation of sepiolite anhydrite.[14] The structural folding is further supported by the reduced peaks at 23.5° and 20.8°, with the respective d-spacing decreasing from 0.378 to 0.376 nm and from 0.441 to 0.439 nm, and the elimination of peaks from 40° to 90°.[1] For the pre-treated sample at 300°C the peak at 31.1° is attributed to dolomite impurities. For samples treated at higher temperatures this peak disappears either due to dolomite's decomposition[14] or the formation of calcite from dolomite's calcination as indicated by the appearance of a new peak at 28.1°.[11]

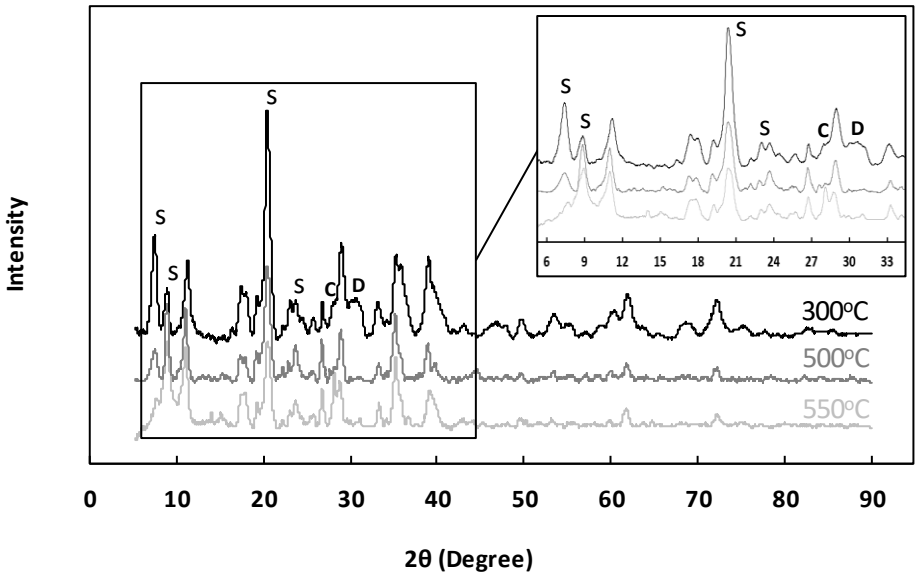

Figure S5. X-ray diffraction patterns of sepiolite samples treated at 300°C, 500°C and 550°C. (S: sepiolite, C: calcite and D: dolomite)

S2. Additional results figures

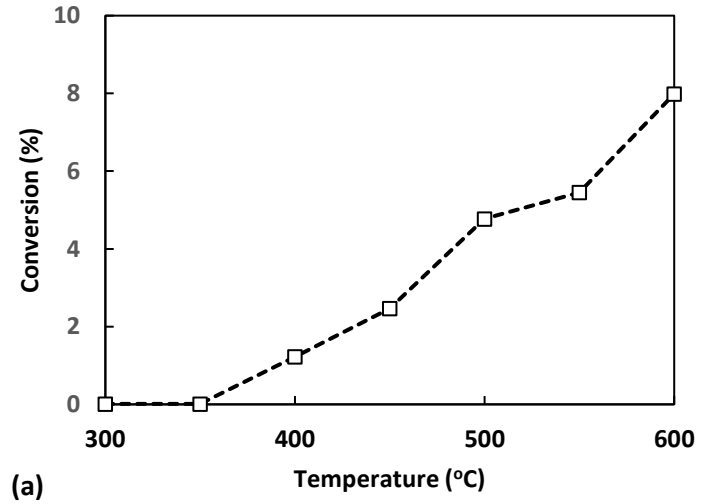

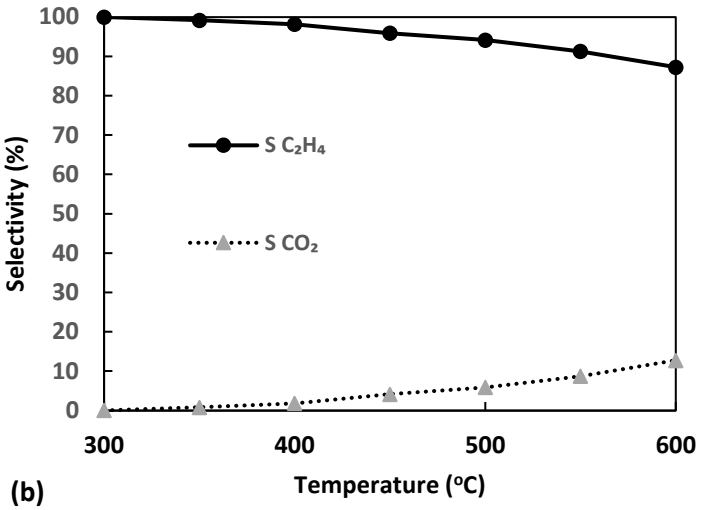

Figure S6. Temperature effect on ethanol conversion (a) and carbon selectivities of CO_2 and C_2H_4 (b) over natural sepiolite. (W/F_{Eth} = 91.8 g_{sep} s g_{Eth}^{-1}, P = 1.7 bar, S/C = 3).

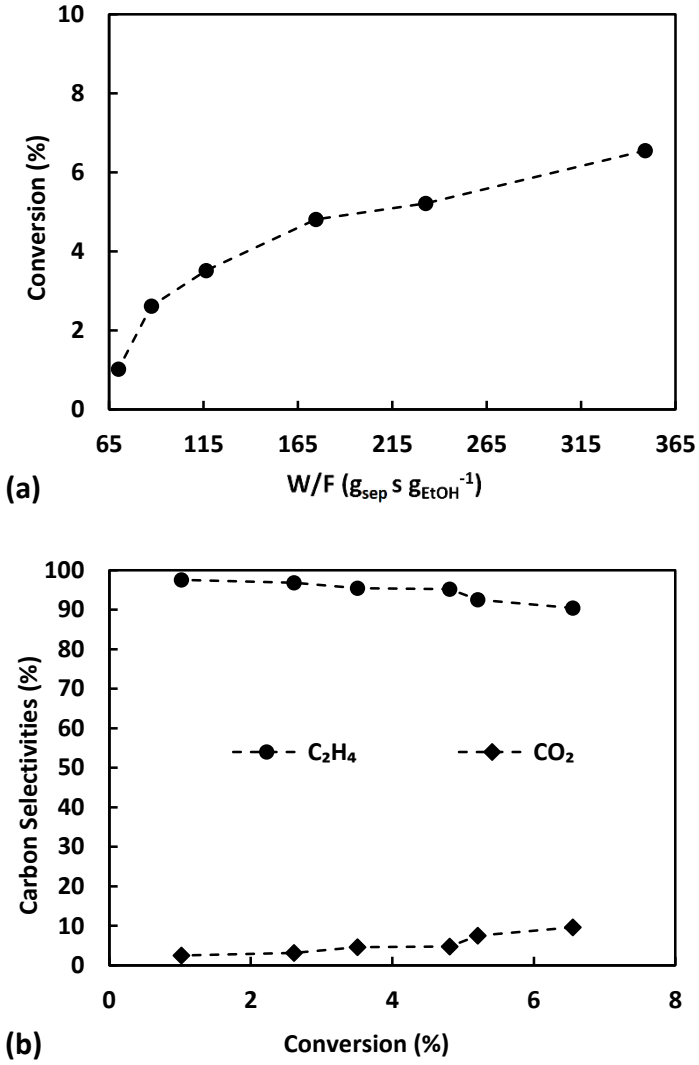

Figure S7. W/F_{t0} effect on ethanol conversion at 400°C (a) and carbon selectivities of CO_2 and C_2H_4 versus ethanol conversion (b) over natural sepiolite. (P = 1.8 bar, S/C = 3).

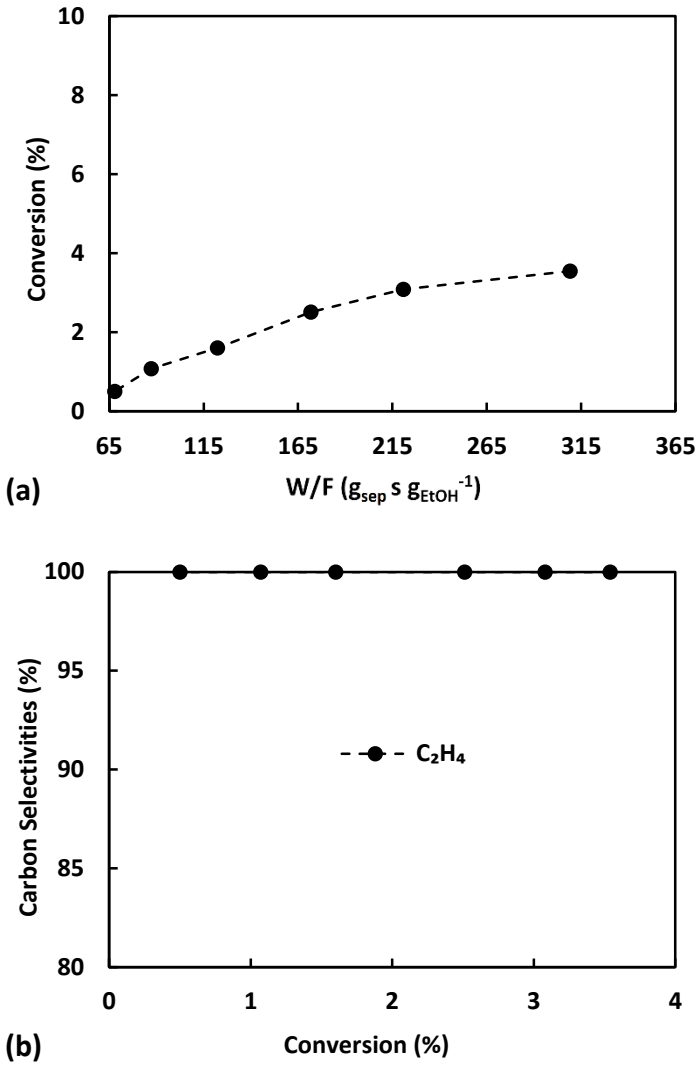

Figure S8. W/F_{t0} effect on ethanol conversion at 400°C (a) and carbon selectivities of C_2H_4 versus ethanol conversion (b) over natural sepiolite. (P = 1.8 bar, S/C = 0).

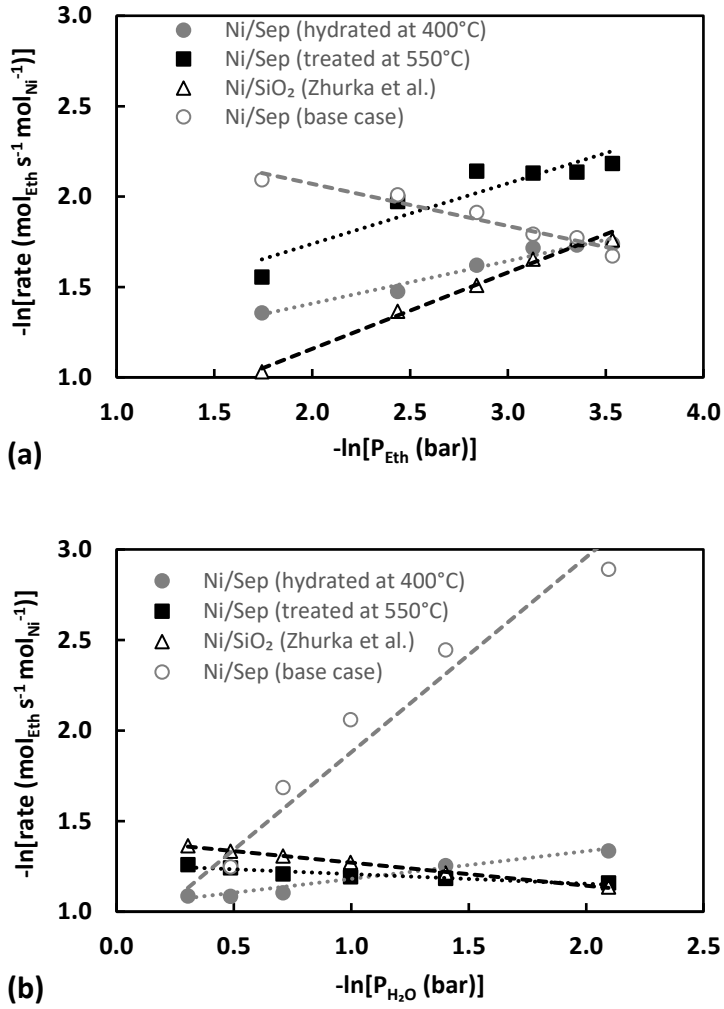

Figure S9. TOF values obtained during ethanol (a) and water (b) partial pressure variation experiments using the base case Ni/Sepiolite catalyst sample treated at 500°C, the thermally pre-treated sample at 550°C, and the hydrated sample at 400°C. TOF values over Ni/SiO_2 from Zhurka et al.[15] are provided for comparison. P_{H_2O} variation experiments carried out at constant P_{Eth} of 0.13 bar, while P_{Eth} variation experiments carried out at constant P_{H_2O} of 0.74 bar.

S3. Bibliography

1 S. Hojati and H. Khademi, Thermal Behavior of a Natural Sepiolite from Northeastern Iran, *J Sci*, 2013, **24**, 129–134.

2 H. Yalçin and Ö. Bozkaya, Ultramafic-rock-hosted vein sepiolite occurences in the Ankara ophiolitic mélange, Central Anatolia, Turkey, *Clays Clay Miner*, 2004, **52**, 227–239.

3 S. Balci, Thermal decomposition of sepiolite and variations in pore structure with and without acid pre-treatment, *Journal of Chemical Technology and Biotechnology*, 1996, **66**, 72–78.

4 M. Önal, H. Yilmaz and Y. Sarikaya, Some physicochemical properties of the white sepiolite known as pipestone from Eskişehir, Turkey, *Clays Clay Miner*, 2008, **56**, 511–519.

5 J. Anderson, S. Falconer and M. Galán-Fereres, Ni/sepiolite hydrogenation catalysts Part 1: Precursor–support interaction and nature of exposed metal surfaces, *Spectrochim Acta A Mol Biomol Spectrosc*, 1997, **53**, 2627–2639.

6 J. A. Anderson and M. Galan-Fereres, Precursor-support interactions in the preparation of sepiolite-supported Ni and Pd catalysts, *Clay Miner*, 1999, **34**, 57–66.

7 A. R. Türker, H. Bağ and B. Erdoğan, Determination of iron and lead by flame atomic absorption spectrometry after preconcentration with sepiolite, *Fresenius J Anal Chem*, 1997, **357**, 351–353.

8 N. Güngör, I. Sevim, E. Günister, H. Teterycz and R. Klimkiewicz, Characterization of sepiolite as a support of silver catalyst in soot combustion, 2006, **32**, 291–296.

9 Y. Grillet, J. M. Cases, M. Francois, J. Rouquerol and J. E. Poirier, Modification of the Porous Structure and Surface Area of Sepiolite Under Vacuum Thermal Treatment, *Clays Clay Miner*, 1988, **36**, 233–242.

10 C. Serna, J. L. Ahlrichs and J. M. Serratosa, Folding in sepiolite crystals, *Clays Clay Miner*, 1975, **23**, 452–457.

11 H. Nagata, S. Shimoda and T. Sudo, On dehydration of bound water of sepiolite, *Clays Clay Miner*, 1974, **22**, 285–293.

12 J. A. Anderson, M. T. Rodrigo, L. Daza and S. Mendioroz, Influence of the support in the selectivity of nickel/clay catalysts for vegetable oil hydrogenation, *Langmuir*, 1993, **9**, 2485–2490.

13 Z. A. Alothman, A review: Fundamental aspects of silicate mesoporous materials, *Materials*, 2012, **5**, 2874–2902.

14 N. Yener, M. Önal, G. Üstünışık and Y. Sarıkaya, Thermal behavior of a mineral mixture of sepiolite and dolomite, *J Therm Anal Calorim*, 2007, **88**, 813–817.

15 M. D. Zhurka, A. A. Lemonidou, J. A. Anderson and P. N. Kechagiopoulos, Kinetic analysis of the steam reforming of ethanol over Ni/SiO_2 for the elucidation of metal-dominated reaction pathways, *React Chem Eng*, 2018, **3**, 883–897.

Bifunctional mechanism proposed for the steam reforming of ethanol over Ni supported on natural sepiolite. The availability of silanols determines the activation of reactants on sepiolite's surface and their migration to the metal-support interface.